N O T I C E

THIS DOCUMENT HAS BEEN REPRODUCED FROM
MICROFICHE. ALTHOUGH IT IS RECOGNIZED THAT
CERTAIN PORTIONS ARE ILLEGIBLE, IT IS BEING RELEASED
IN THE INTEREST OF MAKING AVAILABLE AS MUCH
INFORMATION AS POSSIBLE

FINAL REPORT
June 1978 - June 1980

ACTIVE DAMPING OF MODAL VIBRATIONS
BY FORCE APPORTIONING

William L. Hallauer Jr.
Department of Aerospace and Ocean Engineering
Virginia Polytechnic Institute and State University
Blacksburg, Virginia   24061

TABLE OF CONTENTS

FINAL REPORT

ACTIVE DAMPING OF MODAL VIBRATIONS BY FORCE APPORTIONING[*]

I. INTRODUCTION

The objectives of this research have been to develop and to evaluate by analysis and numerical simulation a method of active structural damping known as force apportioning. This method is based upon the method used in modal vibration testing of isolating modes by multiple-shaker excitation. For either application, active excitation or active damping, one chooses a distribution of as few forces as possible on the structure which will maximally affect selected vibration nodes while minimally exciting all other modes.

NASA sponsorship of this research has fully supported the production of (1) a technical paper presented at a major conference and published in the proceedings (and presently under review for journal publication) and (2) a Master's degree thesis. NASA sponsorship has also partially supported the production of a second Master's degree thesis, which is indirectly related to the principal objectives of this research. Descriptions and bibliographical references to these reports are given in Section II.

During the last few months of the project, additional work was completed which has not previously been reported in writing. The results of this work, which dealt primarily with imperfection sensitivity of the active damping method, are summarized in Section III and are presented in more detail in appendices.

A final oral report was presented by the Principal Investigator at NASA Langley Research Center on July 18, 1980.

---

[*]The NASA Technical Officer for this grant is Mr. Robert Miserentino, NASA Langley Research Center.

II. SUMMARY OF ACCOMPLISHMENTS, AND REPORT REFERENCES

II.A The Basic Form of Active Damping by Force Apportioning

This subject has been described in great detail in a Master's degree thesis [1][*] and in a conference technical paper [2]. Reference 2 is included as Appendix A of this report.

The paper has also been submitted for journal publication. In the journal paper, Section V of Ref. 2 will be simplified considerably. It happens that the same force apportioning vector can be derived with a much more direct approach not requiring the intermediate introduction of a condensed model. The new derivation is included in Appendix B of this report.

II.B The Dynamic Stiffness Method for Plane Grillages

This method, which has been discussed in the Semi-Annual Reports for this project, is the subject of a recent Master's degree thesis [3]. NASA sponsorship supported a part of the theoretical development and computer implementation reported in Ref. 3. A technical paper describing this work will soon be submitted for publication in the Journal of Sound and Vibration.

The method provides exact vibration modes for plane grillage structures, rather than the approximate modes which result from finite element discretization. We had originally planned to use these exact modes in numerical simulations of active damping, such as those described in Section VI of Ref. 2. However, as the project termination date approached, it became clear that the additional time and effort required to employ the exact modes, as opposed to finite element modes, would have no affect on the ultimate conclusions relative to active damping. So the dynamic stiffness method was not employed in the study of

[*]Bracketed numbers refer to the References section.

active damping. However, the dynamic stiffness method itself has considerable intrinsic value, so our efforts in developing and reporting it have been worthwhile.

III.   SUMMARY OF STUDIES NOT PREVIOUSLY REPORTED

III.A. Accuracy of Numerical Simulations of Active Damping

Since modal series truncation and Runge-Kutta integration were used in the time history simulations described in Section VI of Ref. 2, the results are not numerically exact. In order to check the accuracy of the numerical solutions for several cases, we varied the number of modes retained and/or the integration step size from the values stated in Ref. 2. In all cases but one, these variations produced insignificant changes in the results. The one exception was a case in which the integration step size was clearly too long relative to the periods of the high-frequency modes retained; an oscillatory instability resulted which we feel was a numerical artifact and not a qualitatively correct solution of the equations of motion.

III.B. Active Damping of Higher-Frequency Modes

Previous numerical simulations [1,2] have demonstrated only that the lowest flexible modes of a structure can be suppressed effectively, but these new results show that force apportioning is applicable also to the damping of higher-frequency modes. The results are presented in detail in Appendix C.

III.C. Some Studies of Imperfection Sensitivity

Previous reports [1,2] have described active damping by force apportioning under idealized conditions. Numerical simulations have shown that the method can be very effective provided that all necessary modal parameters of the

3

structure are known exactly and that sensors, actuators, and narrow-band filters have ideal operating characteristics. But the effectiveness of the method under more realistic conditions is a matter of more practical interest, so we have conducted a limited study of the effects of non-ideal conditions. Specifically, we have analyzed the case in which the controlled structure's modal parameters are known only approximately and the case of non-ideal frequency filtering.

III.C.1 Inexact Modal Parameters for the Controlled Structure

It has been assumed in previous reports [1,2] that the exact modal parameters were known for the purpose of computing the ideal force apportioning, which is given in Section V of Ref. 2. These new results demonstrate that the effectiveness of the active damping method is not particularly sensitive to somewhat inexact modal parameters, provided that the approximate mode shapes are not drastically different from the actual mode shapes. However, inexact modal information leads to coupling between the controlled modes (those modes denoted by the index s in Eqs. (10) and (15) of Ref. 2), which produces the possibility of long-term system instability. The effects of inexact modal information are described in more detail in Appendix D.

III.C.2 Non-Ideal Frequency Filtering

It has been assumed in previous reports [1,2] that the narrow-band filters required by the active damping method have ideal operating characteristics, namely, infinitely narrow pass-bands and infinitely steep rolloff rates, so that only the desired frequency components are passed. The new results account for filters having finite pass-bands and finite rolloff rates. Numerical simulation results show that the method's effectiveness in suppressing initially existing vibrations in the controlled modes is quite insensitive to

4

typical filter characteristics. However, non-ideal filters do introduce the possibility of long-term system instability due to coupling between all modes, both controlled and uncontrolled. The effects of non-ideal filters are described in more detail in Appendix E.

IV. SUMMARY OF COMPUTER PROGRAMS PREPARED

The computer programs developed for this research are run on the main computers of the VPI&SU Computing Center, an IBM 3032 Processor Complex, and an IBM System 370 Model 158. The IBM 3032 runs the OS/VS2 MVS (Multiple Virtual Storage) operating system with JES2 (Job Entry Subsystem 2) as job scheduler. The IBM 370 runs under the control of Virtual Machine Facility/370 (VM/370); under VM, the Conversational Monitor System (CMS) provides interactive time-sharing support to users at remote terminals. The Computing Center provides Fortran subroutines of the International Mathematics and Statistics Library (IMSL). Automated plotters used for this research are the Versatec 1200 electrostatic plotter (for quick, inexpensive plots) and the Calcomp 1051 drum plotter (for finished ink plots on vellum, suitable for publication).

All programs developed for this research are coded in Fortran IV and compiled by the Fortran H Extended Compiler. With one exception[*], all programs are run with IBM single precision arithmetic. Two types of programs have been written: calculation programs and plotting programs.

The calculation programs generate mass and stiffness matrices for finite element models of plane grillage structures, perform modal eigensolutions,

[*]The exception is EIGENR, the locally developed and undocumented eigensolution subroutine used to calculate modes of small finite element models. EIGENR uses IBM double precision arithmetic.

5

and do time history numerical simulations of active damping. All calculation programs are run from CMS on the IBM 370. The time history numerical simulation programs, ACTIV for Coulomb-type damping and VIACDA for viscous-type damping, make extensive use of the interactive mode for entry of data and inspection of intermediate results by the user.

Two slightly differing Fortran plotting programs, DES2 and DES3, produce Versatec and Calcomp plots, respectively, of time history numerical simulations. Each program is controlled by a different set of job control language instructions. The plotting programs run under MVS.

Documentation for the programs developed in this research is fairly complete but informal, and it will remain in the possession of the Principal Investigator. Appendix B of Reference 1 presents flow diagrams describing the operation of programs ACTIV and VIACDA prior to incorporation of the additional capabilities described in Section III.C.

The programs are operational at this writing and will be kept operational until approximately six months after publication of the journal version of Ref. 2. At that time, some of the operating programs will be deleted from disk storage, and the source programs will be stored as card decks. The decks will remain in the possession of the Principal Investigator for possible future use.

In their present form, the calculation programs are restricted to analysis of unrestrained plane grillage structures having relatively few degrees of freedom. However, with straightforward modifications, the programs could handle any type of structure. The calculation programs constitute a standalone package, except that ACTIV and VIACDA presently use IMSL subroutines for performing the matrix inversion indicated by Eq. (28) of Ref. 2. However,

6

the matrix to be inverted is usually quite small (10 x 10 or smaller), so a short user-supplied subroutine could be employed with no loss of capability.

The programs permit time history plotting of all physical quantities that a user is likely to desire. The user may plot the response in any degree of freedom, the force produced by any control thruster, and the energy in any mode or combination of modes. Figs. 4-7 of Ref. 2 include examples of each of these types of plots. Although all the time history plots included in this report (others than those in Appendix A) represent total energy (i.e., the energy in all modes), plots of several other physical quantities were generated in each case. Some of these other quantities are very interesting (e.g., the energy in only the uncontrolled modes), but they have been excluded in order to limit the length of this report.

V. SOME POSSIBLE REFINEMENTS OF THIS RESEARCH

The topics discussed in this section are not all of equal significance; they are presented below in random order.

The target mode suppression time t_s is defined by Eqs. (7) and (13) of Ref. 2 as being the time specified for decay of modal coordinate ξ_s to a prescribed level. Comparison of Figs. 4a and 7a of Ref. 2 shows that this definition does not lead to comparable rates of energy decay for viscous and Coulomb types of damping with the same value of t_s. Hindsight strongly suggests that defining t_s on the basis of modal energy decay, rather than modal amplitude decay, would be a more rational approach.

In the development of the mathematically ideal force apportioning vector in Section V of Ref. 2 (and the revised version in Appendix B, Section 1 of this report), the restriction is imposed that the number of control actuators

7

must equal the number of controlled modes, $n_a = m$. This restriction arises from the necessity for inverting a partition of the modal matrix, which must therefore be square. But in actual practice, it will probably be required to control more modes than there are available actuators, $m > n_a$. This practical requirement might be satisfied, within the context of active damping by force apportioning, by calculation of the pseudo-inverse of a non-square matrix. The mathematical details of the pseudo-inverse calculation are presented in Appendix B, Section 2. However, no numerical study has been attempted.

One difficult problem which is encountered in active damping by force apportioning is selection of the control thruster locations so as to minimize residual energy. We have addressed this problem in an _ad hoc_, trial-and-error fashion, as is described concisely in Appendix C of this report and Section VI of Ref. 2, and more extensively in Ref. 1. However, it is probable that a more efficient approach could be devised on the basis of relative values of the inner products of modal vectors and force apportioning vectors. This approach is suggested by the discussion in the sixth paragraph of Section VI of Ref. 2.

Section III.C and Appendices D and E of this report discuss the possibility of system instability occurring if the force apportioning and/or the filtering do not have the mathematically ideal forms. We have investigated this possibility simply by integrating the equations of motion and inspecting the time history plots. It is obvious that a much more sophisticated stability analysis could be conducted. Equations (E.2) in Appendix E are the most general equations of motion, accounting for non-ideal apportioning and/or non-ideal filtering, and they would be the basis for a quantitative stability analysis.

VI. CONCLUDING REMARKS

The concluding remarks in Section VII of Ref. 2 still hold without revision. In addition, we may comment now on the new results presented in Section III and the appendices of this report. These results are fairly convincing evidence that the effectiveness of active damping by force apportioning is not significantly impaired by realistic conditions, as opposed to the idealized conditions considered in Ref. 2.

The study described in this report has been exclusively theoretical and computational. It seems reasonable to conclude on the basis of our results that active damping by force apportioning appears on paper to be a practically feasible method. Further and more definitive evaluation of the method requires an experimental study.

REFERENCES

1. J.-F. M. Barthelemy, "Active Damping of Modal Vibrations by Force Apportioning," Master's thesis, Dept. of Aerospace and Ocean Engineering, Virginia Polytechnic Institute and State University, March 1980.

2. W. L. Hallauer Jr. and J.-F. M. Barthelemy, "Active Damping of Modal Vibrations by Force Apportioning," AIAA Paper No. 80-0806-CP, Proc. of the 21st Structures, Structural Dynamics, and Materials Conference, May 12-14, 1980; Seattle. Submitted for publication to the Journal of Guidance and Control.

3. R. Y. L. Liu, "The Dynamic Stiffness Method for Computing Exact Vibration Modes of Plane Grillage Structures," Master's thesis, Dept. of Aerospace and Ocean Engineering, Virginia Polytechnic Institute and State University, March 1980.

10

ACTIVE DAMPING OF MODAL VIBRATIONS
BY FORCE APPORTIONING

W. L. Hallauer Jr.* and J. -F. M. Barthelemy**
Department of Aerospace and Ocean Engineering
Virginia Polytechnic Institute and State University
Blacksburg, Virginia 24061

ABSTRACT

This paper describes with theory and numerical simulation a method of active structural damping which requires relatively few discrete control thrusters suitably positioned on the structure. For each vibration mode which is to be damped (target mode), a particular apportioning of coherently phased control forces is applied which strongly affects that mode while minimally exciting all other modes. The force apportioning used is that which would tune a target mode if the structure were being shaken in a modal vibration test. In contrast to modal testing, however, the forces are varied temporally so as to dampen, rather than excite, the target mode or modes.

NOTATION

$(.)$	column matrix, vector
$[\ ]^T, (.)^T$	transpose of $[\ ]$, $(.)$
$[(\ )^{cc}], (.)^{cc}$	denotes condensation or partitioning relative to both modes and degrees of freedom (d.o.f.)
$[(\ )^c]$	denotes partitioning relative to modes only
$(u,v) = u^T v$	
$[k]$	n x n stiffness matrix
$[m]$	n x n inertia matrix
$[\phi]$	n x n modal matrix
$[\psi] = [\phi^{cc}]^{-T} = ([\phi^{cc}]^{-1})^T$	
f_s	force apportioning vector for damping of a target mode
ϕ_r	rth column of $[\phi]$, mode shape of rth mode
$Q(t)$	n x 1 action (force and moment) vector
$q(t)$	n x 1 d.o.f. vector
$\xi(t)$	vector of normal or modal coordinates
$\delta_{rs} = \begin{cases} 1, & r = s \\ 0, & r \neq s \end{cases}$	
$M_r = \phi_r^T [m] \phi_r$	generalized mass of the rth mode

* Associate Professor, Member AIAA
**Graduate Research Assistant, Member AIAA

$E_r(t)$	energy in the rth mode
K_s	feedback constant for damping of target mode, Eqs. (8) and (13)
m	number of target modes
n	total number of d.o.f. in structural model
n_c	number of modes and d.o.f. in condensed model
$\omega_{ds} = \omega_s \sqrt{1 - \zeta_s^2}$	
ω_r	natural frequency of the rth mode
P_s	target mode viscous decay criterion, Eq. (7)
r	index denoting an arbitrary mode
s	index denoting a target mode
t	time
t_s	target mode suppression time, Eqs. (7) and (13)
$\xi_{so} = \xi_s(0)$	initial value of target mode normal coordinate
ζ_s	target mode viscous active damping factor

I. INTRODUCTION

To suppress the vibrations caused by operational or environmental conditions, modern vehicle and building structures may require additional damping beyond that provided by inherent passive mechanisms of energy dissipation. The traditional source of artificial damping is a passive device, but for some current applications such devices are ineffective or are unsatisfactory for other reasons, such as excessive weight. For these applications, additional artificial damping might be provided by an active system, i.e. a system which uses sensing, feedback, and control forces or moments to oppose the structural motion.

Herzberg et al.[1] have observed that the well established technology of modal vibration testing is adaptable to the control of structural vibrations. This paper describes a method of active damping which is just such an adaptation.

A possible application of this method is for the suppression of vibrations in proposed large space structures. These structures will be subjected to sources of disturbance such as propulsive

1

11

forces or gyroscopic moments to effect maneuvers, but the vacuum of space will provide no atmospheric damping and it seems likely that internal structural damping will generally be low. The potential significance of active damping for large space structures has inspired a great deal of current research. No literature review will be attempted here, but Ref. 2 includes a number of very recent papers and much bibliographic information on the subject.

Most previous contemporary studies of active structural damping have applied advanced control theory, e.g. the papers of Balas[3] and Meirovitch and Oz[4]. In contrast, the basic form of active damping by force apportioning introduced here involves no control theory beyond the behavior of a one-degree-of-freedom damped oscillator.

II. GENERAL DISCUSSION OF FORCE APPORTIONING

The traditional application of force apportioning is for modal vibration testing with two or more sinusoidally varying, coherently phased mechanical shakers. The shakers are attached to suitable points on the structure being tested, and their force amplitudes are apportioned in such a way as to tune a selected vibration mode, which we call the target mode. Ideally, all of the energy is fed into the target mode at its natural frequency, and all other modes, which we call the residual modes, are untouched. This focusing of energy into a single mode is attributable to the specific spatial distribution of shakers and their relative force amplitudes.

In reality, perfect tuning is generally not possible with a finite number of shakers. The practical objective of modal testing with force apportioning is to tune with as few shakers as possible while still minimizing excitation of residual modes so that target mode parameters can be accurately measured. Several methods have been developed or proposed for calculating the apportioning of shaker force amplitudes to produce effective mode tuning, e.g. the methods of Lewis and Wrisley[5], Asher[6], Ibanez[7], and Morosow and Ayre[8].

In modal vibration testing, the properly apportioned forces feed energy into the target mode and stimulate motion by virtue of being in phase with the velocity of target mode response. Conversely, for active damping of existing but unwanted vibration in a target mode, the same spatial distribution and apportioning of forces, but 180° out of phase with the velocity, will extract energy from that mode. The target mode or modes can always be suppressed in this manner, but a possible undesirable byproduct is the pumping of energy into residual modes. Successful application of this method of active damping requires that the control force locations be chosen so as to minimize residual energy. This point is discussed in more detail subsequently.

To describe force apportioning mathematically, we write the equations of motion for a linear structure discretized to n degrees of freedom (d.o.f.),

$$[m] \, \ddot{q} + [k] \, q = Q \qquad (1)$$

Internal passive structural damping is omitted to simplify the analysis.* We denote a target mode as mode s, and the vector of coherently phased actions (forces and moments) which selectively affects mode s as $Q_s(t)$. Substituting into Eq. (1) Q_s and the standard normal mode transformation

$$q(t) = [\phi] \, \xi(t) = \sum_{r=1}^{n} \phi_r \, \xi_r(t) \qquad (2)$$

leads, with mass and stiffness orthogonality conditions, to the modal equations of motion,

$$M_r \ddot{\xi}_r + M_r \omega_r^2 \, \xi_r = (\phi_r, Q_s), \quad r = 1,2,\ldots,n \quad (3)$$

The mathematical objective of force apportioning is to select the constant shape f_s of $Q_s(t)$ so as to maximize generalized force (ϕ_s, Q_s) into the target mode while minimizing generalized forces (ϕ_r, Q_s), $r \neq s$, into all residual modes, thus minimizing residual responses, $\xi_r(t)$; $r \neq s$. Existing methods[5-8] for calculating f_s have been developed primarily for application with experimental transfer function data. For purposes of this study, however, we present in Section V a simpler method which requires a priori knowledge of modal parameters.

In the next section, expressions for $Q_s(t)$ are developed (with f_s left unspecified) leading to standard viscous and Coulomb types of modal damping.

III. ARTIFICIAL VISCOUS AND COULOMB
TYPES OF DAMPING

From Eq. (2), the portion of response in any particular d.o.f. i due to mode s is

$$q_{is}(t) = \phi_{is} \, \xi_s(t) \qquad (4)$$

We specify that motion $q_i(t)$ of a single selected translation, the ith d.o.f., is measured by a sensor, typically an accelerometer, and that the quantity $q_{is}(t)$ for each target mode is produced from $q_i(t)$ by narrow-band filtering around the target mode natural frequencies.

III.A Artificial Viscous Damping

To produce simple viscous type damping in a single target mode, we specify

$$Q_s = -K_s \, f_s \, \dot{q}_{is} \qquad (5)$$

where K_s is a feedback constant to be determined. Thus, modal equations (3) become

*Note, however, that the actual structural damping of large space structures is likely to be slight. If so, it will produce negligible coupling of the undamped normal modes[9] and, therefore, can only complement, rather than detract from, the damping provided by artificial means. Thus, the neglect of natural damping in the analysis should, for large space structures, lead to conservative results.

$$M_r\ddot{\xi}_r + M_r\omega_r^2\xi_r = -K_s(\underline{\phi}_r,\underline{f}_s)\ \phi_{is}\ \dot{\xi}_s, \quad (6)$$

$$r = 1,2,\ldots,n$$

In the numerical simulations of Section VI, non-zero initial displacement and zero initial velocity are specified for each target mode, and it is required that each target mode exponential decay envelope be damped to a portion $p_s \ll 1$ of its initial value in time t_s. Thus, the required viscous damping factor is

$$\zeta_s = \frac{\ell n(1/P_s)}{\omega_s t_s} \quad (7)$$

and, from the sth equation of (6), the feedback constant is

$$K_s = \frac{2\ M_s\ \omega_s\ \zeta_s}{(\underline{\phi}_s,\underline{f}_s)\ \phi_{is}} \quad (8)$$

If a number m of target modes are to be damped simultaneously, then the appropriate action vector is

$$\underline{Q}(t) = -\sum_{s=1}^{m} K_s\ \underline{f}_s\ \dot{q}_{is} \quad (9)$$

In Eq. (9), we assume for simplicity that the m target modes are the first m modes of the structure, but in general the target modes need not be only the lowest modes, nor need they be a series of consecutive modes. With Eq. (9), the modal equations become

$$M_r\ddot{\xi}_r + M_r\omega_r^2\xi_r = -\sum_{s=1}^{m} K_s(\underline{\phi}_r,\underline{f}_s)\ \phi_{is}\ \dot{\xi}_s, \quad (10)$$

$$r = 1,2,\ldots,n$$

where K_s for each target mode is calculated from Eqs. (7) and (8). Figure 1* is a conceptual block diagram illustrating the implementation of Eq. (10) for active damping of two modes of a discretized beam, with the use of three control thrusters. For simultaneous damping of more than one mode, as in Fig. 1, the elements of apportioning vectors f_s, $s = 1,2,\ldots,m$, can be represented as elements of a rectangular matrix.

Artificial viscous damping requires that the control forces be continuously variable in time, and it leads to a mathematically linear problem. It is possible, though, that propulsive control units will not be capable of delivering continuously variable thrust. So we consider next a type of control force which perhaps is more likely to be achieved in practice, but leads to a nonlinear problem.

III.B Artificial Coulomb Damping

To produce damping similar to Coulomb damping[10] in a single target mode, we specify

$$\underline{Q}_s = -K_s\ \underline{f}_s\ \text{sgn}(\dot{q}_{is}) \quad (11)$$

where

$$\text{sgn}(.) = \begin{cases} 1 & \text{for} \quad (.) > \epsilon_v \\ 0 & \text{for} \quad |(.)| \leq \epsilon_v \\ -1 & \text{for} \quad (.) < -\epsilon_v \end{cases}$$

and ϵ_v is a threshold velocity level, which is zero for pure Coulomb damping. Small $\epsilon_v > 0$ is considered here because any actual propulsive device must shut off at some non-zero level of command signal. Equation (11) is an approximation to the type of propulsive thrust often referred to as "bang-bang" (or "on-off") thrust with a deadband[4]. With Eqs. (4) and (11), modal equations (3) become

$$M_r\ddot{\xi}_r + M_r\omega_r^2\ \xi_r = -K_s(\underline{\phi}_r,\underline{f}_s)\ \text{sgn}(\phi_{is}\dot{\xi}_s), (12)$$

$$r = 1,2,\ldots,n$$

With the initial value of target mode displacement in the ith d.o.f. specified as $q_{is}(0) = \xi_s(0)/\phi_{is}$ and zero initial velocity, we require that mode s be suppressed in time t_s. Provided that ϵ_v is small relative to peak target mode velocities, the feedback constant K_s which will give suppression time t_s is calculated as follows. For pure Coulomb damping $(\epsilon_v = 0)$, decay per period $2\pi/\omega_s$ of $\xi_s(t)$ in the sth equation of (12) is[10]

$$\frac{4\ K_s\ (\underline{\phi}_s,\underline{f}_s)}{M_s\ \omega_s^2}\ \frac{\phi_{is}}{|\phi_{is}|}$$

The initial amplitude $|\xi_s(0)|$ equals the decay per period times the number of periods to suppression, $\omega_s t_s/2\pi$. Thus, a little algebra gives

$$K_s = \frac{\pi}{2}\ \frac{M_s\omega_s|q_{is}(0)|}{t_s\ (\underline{\phi}_s,\underline{f}_s)\phi_{is}} \quad (13)$$

If a number m of target modes are to be damped simultaneously, then the appropriate action vector is

$$\underline{Q}(t) = -\sum_{s=1}^{m} K_s\underline{f}_s\ \text{sgn}(\dot{q}_{is}) \quad (14)$$

and the modal equations become

$$M_r\ddot{\xi}_r + M_r\omega_r^2\xi_r = -\sum_{s=1}^{m} K_s(\underline{\phi}_r,\underline{f}_s)\ \text{sgn}(\phi_{is}\dot{\xi}_s), (15)$$

$$r = 1,2,\ldots,n$$

where K_s for each target mode is calculated from Eq. (13).

It should be noted that for small ϵ_v the individual control forces for single-mode damping, Eq. (11), will vary with time in nearly a square wave. However, because a number of nearly square waves are being superimposed in Eq. (14), the time variation of each control force for multi-mode damping generally will have the character of erratic stairsteps. This is illustrated in Section VI.

IV. SPECIAL CASE: VISCOUS DAMPING
OF ONE TARGET MODE

This relatively simple case is amenable, in part, to closed-form solution. The solution obtained will provide useful information which is applicable, at least qualitatively, to the analysis of more complicated cases.

We seek solutions of modal equations (6) with feedback constant (8). The sth modal equation is rewritten as

$$\ddot{\xi}_s + 2\zeta_s \omega_s \dot{\xi}_s + \omega_s^2 \xi_s = 0$$

and we specify initial conditions $\xi_s(0) = \xi_{so} \neq 0$ and $\dot{\xi}_s(0) = 0$. The solution is

$$\xi_s(t) = \xi_{so}(\omega_s/\omega_{ds})e^{-\zeta_s\omega_s t} \cos(\omega_{ds}t + \theta_s) \quad (16)$$

where

$$\omega_{ds} = \omega_s \sqrt{1 - \zeta_s^2}$$

$$\theta_s = \tan^{-1}(-\zeta_s\omega_s/\omega_{ds})$$

Next we substitute Eq. (16) into the right-hand sides of all residual $(r \neq s)$ modal equations of (6) and, again using Eq. (8), find the non-homogeneous equations

$$M_r\ddot{\xi}_r + M_r\omega_r^2\xi_r = C_{rs}e^{-\zeta_s\omega_s t}\sin\omega_{ds}t, \quad r \neq s \quad (17)$$

where

$$C_{rs} = \frac{2 M_s\omega_s^2 \zeta_s \xi_{so}}{\sqrt{1 - \zeta_s^2}} \frac{(\phi_r \cdot f_s)}{(\phi_s \cdot f_s)}$$

With initial conditions $\xi_r(0) = 0$ and $\dot{\xi}_r(0) = 0$ for $r \neq s$, the solution of Eq. (17) can be written as a convolution integral,

$$\xi_r(t) = \frac{C_{rs}}{M_r\omega_r} \int_0^t e^{-\zeta_s\omega_s\tau}\sin\omega_{ds}\tau\sin\omega_r(t-\tau)d\tau \quad (18)$$

Equations (16) and (17) show that the target mode eventually decays and excitation of the residual modes eventually ceases. But after the target mode is suppressed, the residual modes remain in a steady state of free vibration. This steady-state motion can be determined by setting the upper limit in integral (18) to infinity, which also makes the integral reasonably tractable. The result of this evaluation has the form

$$\xi_r^{ss}(t) = \bar{\xi}_r \cos(\omega_r t + \theta_r) \quad (19)$$

where $\bar{\xi}_r$ and θ_r are algebraically complicated.

Rather than examining amplitude $\bar{\xi}_r$, it is perhaps more useful to evaluate the residual energy, which is a significant global quantity. The instantaneous energy in any mode is

$$E_r(t) = \frac{1}{2} M_r(\dot{\xi}_r^2 + \omega_r^2 \xi_r^2) \quad (20)$$

Thus, the ratio of steady-state residual mode energy to initial energy is found to be

$$\frac{E_r^{ss}}{E_s(0)} = \frac{M_r\omega_r^2 \bar{\xi}_r^2}{M_s\omega_s^2 \xi_{so}^2}$$

$$= \frac{4 \zeta_s^2 \frac{M_s}{M_r} (\frac{\omega_s}{\omega_r})^4 \left[\frac{(\phi_r \cdot f_s)}{(\phi_s \cdot f_s)}\right]^2}{\left[1 - (\frac{\omega_s}{\omega_r})^2\right]^2 + \left[2\zeta_s \frac{\omega_s}{\omega_r}\right]^2} \quad (21)$$

Equation (21) demonstrates that selection of an active damping factor ζ_s involves a compromise: a higher ζ_s is desirable to suppress the target mode more rapidly, but a lower ζ_s is desirable to minimize residual energy. Equation (21) also shows that residual modes with frequencies somewhat greater than that of the target mode are relatively immune to excitation, the residual energy varying nearly as the fourth power of the frequency ratio. On the other hand, residual modes with frequencies lower than that of the target mode are not protected by a favorable frequency ratio and seem somewhat susceptible. In the limit as ω_r goes to zero, Eq. (21) gives the residual energy remaining in a rigid body mode,

$$\left[\frac{E_r^{ss}}{E_s(0)}\right]_{rb} = 4 \zeta_s^2 \frac{M_s}{M_r}\left[\frac{(\phi_r \cdot f_s)}{(\phi_s \cdot f_s)}\right]^2 \quad (22)$$

Equation (22) shows that force apportioning vector f_s must be orthogonal to all rigid body mode shapes in order not to disturb the structure's rigid body orientation.

V. FORCE APPORTIONING BASED ON A
CONDENSATION TECHNIQUE

We first establish an apportioning of forces and moments which is applicable to the full discretized structural model characterized by Eq. (1). To isolate the sth mode from all others, we set

$$g_s = [m] \phi_s g(t)$$

where $g(t)$ is an arbitrary function of time. Then modal equations (3) become

$$M_r\ddot{\xi}_r + M_r\omega_r^2 \xi_r = M_s \delta_{rs} g(t), \quad r = 1,2,\ldots n$$

where δ_{rs} is the Kronecker delta. Thus, the ideal apportioning of forces and moments is

$$f_s = [m] \phi_s \quad (23)$$

But Eq. (23) implies the presence of a control force or moment at each d.o.f. of the structure, which is generally impossible. So we develop next a condensed, or reduced order, mathematical model of the structure, for which an apportioning analogous to Eq. (23) can be defined.

The condensed model is required to include $n_c < n$ translation d.o.f. corresponding to control

thrusters and to preserve without alteration n_c selected modes of the structure. Accordingly, we define the $n_c \times n_c$ condensed inertia and stiffness matrices by analogy with the standard orthogonality conditions,

$$[\phi^{cc}]^T[m^{cc}][\phi^{cc}] = \lceil M^c \rfloor$$
$$[\phi^{cc}]^T[k^{cc}][\phi^{cc}] = \lceil \omega^2 M^c \rfloor \qquad (24)$$

where $[\phi^{cc}]$ is the $n_c \times n_c$ partition of the full modal matrix $[\phi]$ containing only the d.o.f. and modes to be retained in the condensed model, and $\lceil M^c \rfloor$ and $\lceil \omega^2 M^c \rfloor$ are the $n_c \times n_c$ partitions of the generalized mass and stiffness matrices, respectively containing only parameters of the retained modes. Provided that $[\phi^{cc}]$ is not singular, the condensed inertia matrix is therefore

$$[m^{cc}] = [\phi^{cc}]^{-T} \lceil M^c \rfloor [\phi^{cc}]^{-1} \qquad (25)$$

and $[k^{cc}]$ is calculated similarly.

Thus, the condensed version of Eq. (1) is

$$[m^{cc}] \, \ddot{q}^c + [k^{cc}] \, q^c = Q^c \qquad (26)$$

where q^c and Q^c are the partitions of q and Q, respectively, which contain only the translation d.o.f. and the associated forces retained in the condensed model. It can be proved[11] that problem (26) preserves exactly the modal parameters and the free and forced response of the retained modes and d.o.f.

In analogy with Eq. (23), we define a condensed force apportioning vector which completely isolates mode s from all other modes retained in the condensed model,

$$f_s^{cc} = [m^{cc}] \, \phi_s^{cc} \qquad (27)$$

To simplify Eq. (27), we define in Eq. (25)

$$[\psi] = [\phi^{cc}]^{-T} \text{ or } (\psi_r, \phi_s^{cc}) = \delta_{rs} \qquad (28)$$

Substituting Eqs. (25) and (28) into (27) then gives

$$f_s^{cc} = M_s \, \psi_s \qquad (29)$$

The constant M_s in Eq. (29) is irrelevant since, in calculations, f_s^{cc} is normalized to a maximum element value of ± 1, as are all mode shape vectors. The $n_c \times 1$ vector f_s^{cc} is the non-zero partition of the full $n \times 1$ apportioning vector f_s, all remaining elements of f_s being set to zero. Since $(\psi_r, f_s) = M_s \delta_{rs}$ for all modes retained in the condensed model, this apportioning will control the target mode without affecting the other retained modes. But, in general, it will excite the modes which have not been included in the condensed model. When used in Eqs. (10) or (15), this apportioning completely controls n_c selected modes with n_c selected control thrusters (provided that $[\phi^{cc}]$ is not singular), but all other residual modes are uncontrolled. An important objective in control thruster selection, therefore, is to minimize excitation of uncontrolled modes.

The condensation-apportioning procedure described in this section requires complete information on the modes to be retained in the reduced order model, and it assures that each of the retained modes can be isolated from all other retained modes. On the other hand, apportioning techniques used in modal testing[5-8] do not require modal parameters a priori, but they also do not produce any assured measure of mode isolation. So Eq. (29) probably represents the mathematically best apportioning of a limited number of control thrusters, but it may not be best in practice because it requires previously determined modal parameters.

VI. NUMERICAL SIMULATIONS OF ACTIVE DAMPING

Time history simulations have been calculated for evaluation of active damping by force apportioning, the performance measure of interest being the residual energy remaining after the target modes are suppressed.

Figure 2 depicts the unrestrained plane grillage structural model used in the simulations. It is a relatively simple mathematical model designed to exhibit structural dynamic characteristics typical of proposed solar power satellites[12], in particular, low natural frequencies and high modal density. The model is an assemblage of straight bending-torsion beam finite elements with twelve nodes, as numbered in Fig. 2. Each node has a translational d.o.f. in the Z direction and rotational d.o.f. about the X and Y directions, for a total of 36 d.o.f. Accordingly, the model has a rigid body translation mode in the Z direction and rigid body rotation modes about the X and Y directions. Each of the six square bays has side length $L = 4000$ m. A mass of 4.8×10^5 kg (10% of the total mass of beams) with rotational inertias of 3.0×10^{10} kg $\cdot$ m² is concentrated at node 2. Inertias of the beam elements are represented by consistent mass matrices. Each element has mass per unit length of 35.3 kg/m, torsional inertia per unit length of 5.65×10^4 kg $\cdot$ m, bending stiffness EI of 7.55×10^{12} N $\cdot$ m², and torsional stiffness GJ of 5.81×10^{12} N $\cdot$ m². Natural frequencies and periods of the first eleven flexible modes are listed in Table 1. Mode shapes of the first six flexible modes are shown in Figs. 3.

For each simulation, the target modes selected were modes 4 - 6, the first three flexible modes. The only non-zero initial conditions specified were mode 4 initial value $\xi_4(0)$ corresponding to node 1 translation $q_{14}(0) = 1.0$ m, and initial values of $\xi_5(0)$ and $\xi_6(0)$ corresponding to equal initial potential energy in each target mode. The feedback signal chosen was node 1 translation velocity $\dot{q}_1(t)$. In addition to the target modes 4 - 6, rigid body modes 1 - 3 were retained in the condensed model in order to avoid disturbing the rigid body orientaion (cf. Eq. (22)). Six thrusters were required to control these six modes.

In calculations, only the first 14 of the total 36 modes were retained, i.e. Eq. (2) was truncated after $r = 14$. This truncation is justified by the $(\omega_s/\omega_r)^4$ term in Eq. (21) and by the observation that the highest retained modes contributed negligibly to the total response. The modal equations of motion were integrated by a

fourth-order Runge-Kutta method with constant step size (2 s for viscous damping, 1 s for Coulomb).

Active damping performance was evaluated for different control thruster locations, different times to damp the target modes, and different damping types, viscous or Coulomb. Case 1 is the reference case, and the parameters were varied individually for Cases 2 - 4. In Case 1, control thrusters are located at nodes 1, 2, 3, 5, 10, and 12, and damping is viscous with time $t_S =$ 400 s to damp each target mode down to portion $p_S = 0.01$ of its initial value. Time histories for selected quantities are shown in Figs. 4. Individual modal energy values were calculated from Eq. (20) and summed to produce Fig. 4a, the history of total energy. The active damping in this case is very effective, with residual energy being less than 3% of initial energy.

For the damping type and time of Case 1, several combinations of six control thruster locations were investigated. A few combinations cannot be used because the associated $[\phi^{CC}]$ matrices are singular (see Eqs. (28) and (29)), but most can be used[11]. The thruster locations of Case 1 produced one of the best results. For Case 2, a control thruster was moved from node 5 to node 11, and this change produced one of the worst results. Figures 5 show that the active damping is counterproductive: the residual energy is 28 times the initial energy, with 67% of the residual energy remaining in mode 8 alone. This poor performance can be explained by examination of the force apportioning vectors and feedback constants for Cases 1 and 2 (Table 2) and the mode shapes for modes 4 and 8 (Figs. 3 a,e). Equations (10) and (21) suggest that (ϕ_s, f_s) should be large in comparison with (ϕ_r, f_s), $r \neq s$. For target mode 4 and residual mode 8 in Case 1, this condition is satisfied. In Case 2, however, (ϕ_4, f_4) is very small in comparison with (ϕ_8, f_4) and, consequently, K_4 is relatively large and a great deal of energy is pumped into mode 8.

The parameters of Case 3 are those of Case 1, except that damping time is halved, $t_S = 200$ s, so that ζ_S is doubled. Although Eq. (21) suggests that the residual energy might be quadrupled by this increased damping, the actual residual energy in Fig. 6a is only a little more than twice that of Case 1.

The parameters of Case 4 are those of Case 1 except that damping is the Coulomb type, Eq. (14), with $\varepsilon_v = 0.0001$ m/s for all target modes. Figures 7 demonstrate that this damping is very effective. Comparison of Figs. 4c and 7c shows that lower force levels are required for Coulomb type damping, but that these levels must be maintained throughout the damping period. For $t \approx 400$ s, Fig. 7c exhibits thruster chattering, which results from one target mode alternating between free and damped motion around the threshold velocity level.

VII. CONCLUDING REMARKS

The basic form of active vibration damping by force apportioning has been described with standard structural modal analysis and numerical

simulations. For possible application to satellite structures, rigid body modes have been considered, but the influence of gravity on orbital position and attitude has been neglected. Feedback control laws producing modal damping of the simple viscous and Coulomb types have been used.

To permit evaluation of the method in its basic form, only idealized conditions have been considered. It has been assumed that all necessary modal parameters are known and that sensors, actuators, and narrow-band filters have ideal operating characteristics. The damping of two or more modes with effectively identical natural frequencies has not been investigated.

Under these idealized conditions, the method is effective and relatively simple. It uses a single sensor and a limited number of discrete thrusters to control completely an equal number of modes. The significant measure of performance is the amount of residual energy fed into the uncontrolled modes during the process of damping the controlled modes. In the numerical example presented, a judicious choice of control thruster locations and moderate damping of the controlled modes produces only an insignificant amount of residual energy.

REFERENCES

1. R. J. Herzberg, K. F. Johansen, and R. C. Stroud, "Dynamics and Control of Large Satellites," Astronautics & Aeronautics, October 1978, pp. 35-39.

2. Proceedings of the Second VPI&SU/AIAA Symposium on Dynamics and Control of Large Flexible Spacecraft (ed. L. Meirovitch), June 21-23, 1979, Blacksburg, VA.

3. M. J. Balas, "Enhanced Modal Control of Flexible Structures Via Innovations Feedthrough," Reference 2, pp. 677-700, 1979.

4. L. Meirovitch and H. Oz, "Modal-Space Control of Large Flexible Spacecraft Possessing Ignorable Coordinates," Reference 2, pp. 701-727, 1979.

5. R. C. Lewis and D. L. Wrisley, "A System for the Excitation of Pure Natural Modes of Complex Structures," Journal of the Aeronautical Sciences, 17(11), pp. 705-722 and 735, November 1950.

6. G. W. Asher, "A Method of Normal Mode Excitation Utilizing Admittance Measurements," Proceedings of the National Specialists' Meeting on Dynamics and Aeroelasticity, pp. 69-76, Institute of Aeronautical Sciences, Fort Worth, 1958.

7. P. Ibanez, "Force Appropriation by Extended Asher's Method," SAE Paper No. 760873, SAE Aerospace Engineering and Manufacturing Meeting, San Diego, 1976.

8. G. Morosow and R. S. Ayre, "Force Apportioning for Modal Vibration Testing Using Incomplete Excitation," The Shock and Vibration Bulletin, 48 (1), pp. 39-48, 1978.

9. T. K. Hasselman, "Modal Coupling in Lightly Damped Structures," AIAA Journal, 14 (11), pp. 1627-1628, 1976.

10. L. Meirovitch, Elements of Vibration Analysis, Section 1.7, McGraw-Hill, 1975.

11. J. -F. M. Barthelemy, "Active Damping of Modal Vibrations by Force Apportioning," Master's thesis, Dept. of Aerospace and Ocean Engineering, Virginia Polytechnic Institute and State University, March 1980.

12. R. H. Nansen and H. DiRamio, "Structures for Solar Power Satellites," Astronautics & Aeronautics, October 1978, pp. 55-59.

Table 1   Flexible mode natural frequencies and periods for unrestrained plane grillage structure

Mode	Frequency (Hz)	Period (s)
4	0.0062	161.29
5	0.0065	153.85
6	0.0129	77.52
7	0.0143	69.93
8	0.0155	64.52
9	0.0180	55.56
10	0.0217	46.08
11	0.0232	43.10
12	0.0245	40.82
13	0.0448	22.32
14	0.0489	20.45

Table 2   Force apportioning vectors and feedback constants for active damping of mode 4

	Case 1	Case 2
$f_{1,4}$	-0.128	-0.244
$f_{2,4}$	0.923	0.488
$f_{3,4}$	-0.128	-0.244
$f_{5,4}$	-1.000	-
$f_{10,4}$	0.167	0.500
$f_{11,4}$	-	-1.000
$f_{12,4}$	0.167	0.500
K_4(kg/sec)	5.40×10^4	1.54×10^6
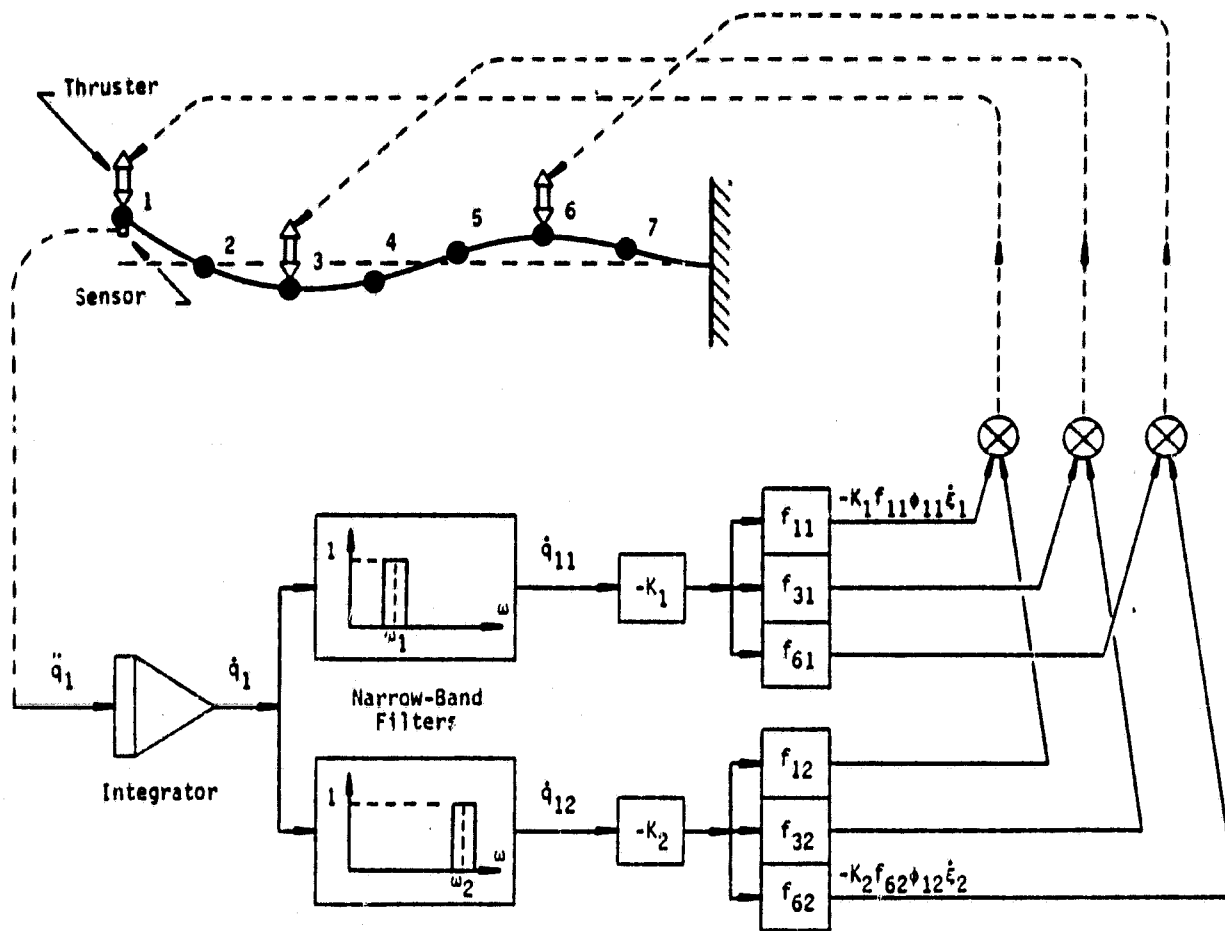
Fig. 1 Force apportioning control system to damp two modes of a discretized cantilevered beam using three thrusters
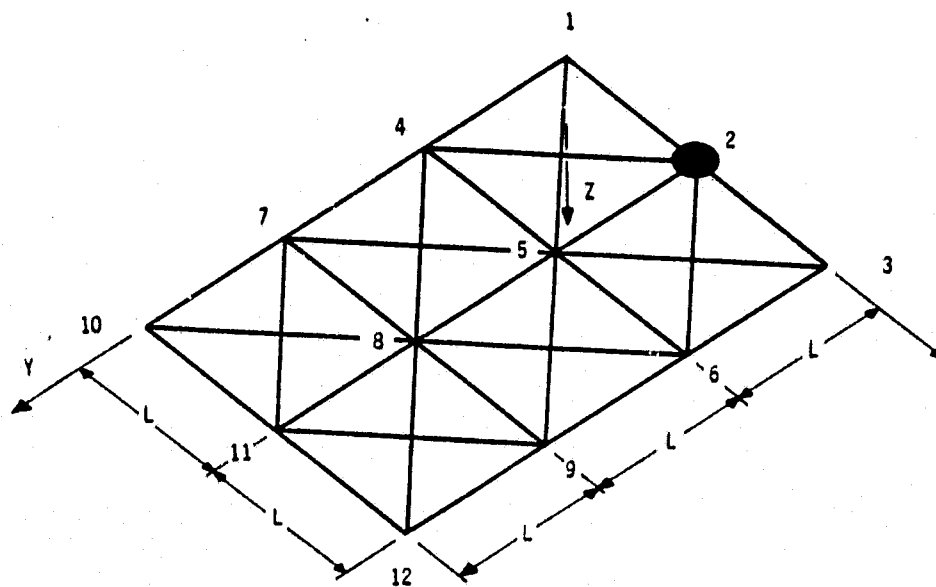
Fig. 2 Unrestrained plane grillage structure
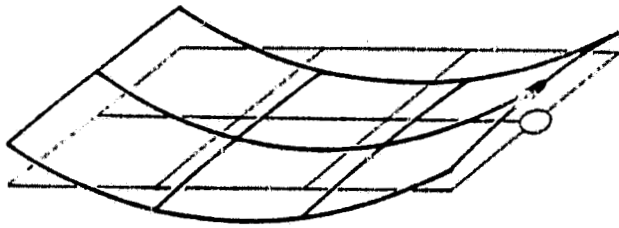
a) Mode 4
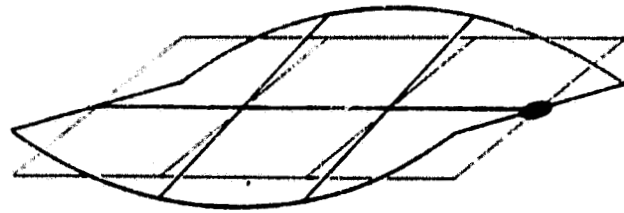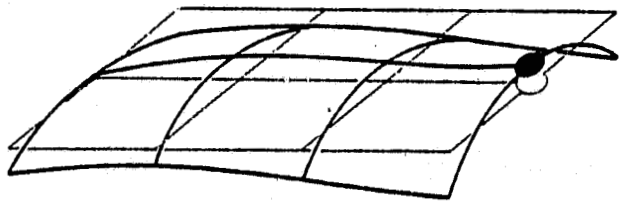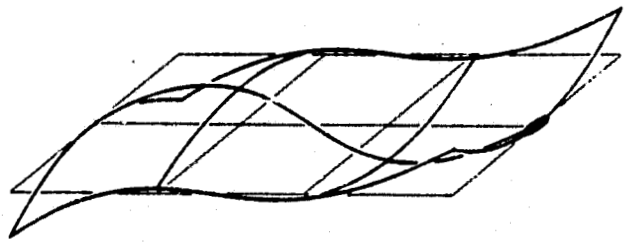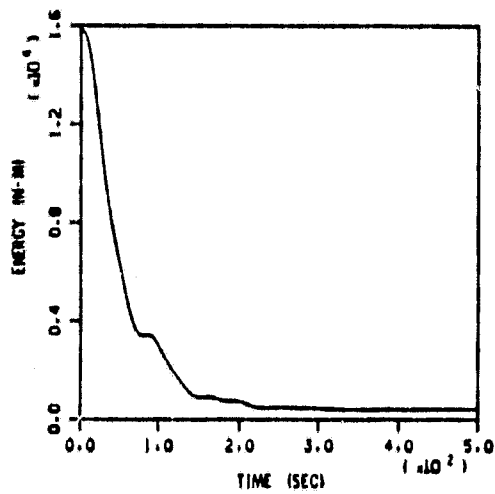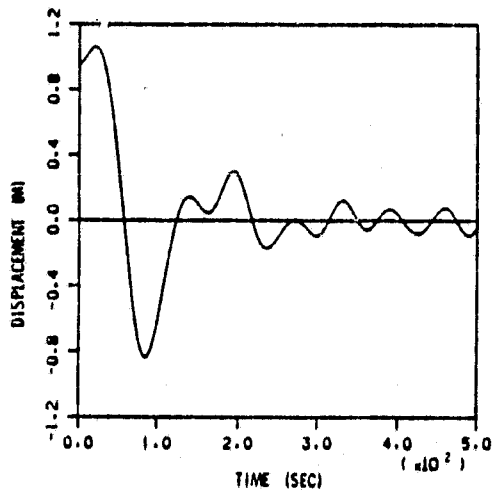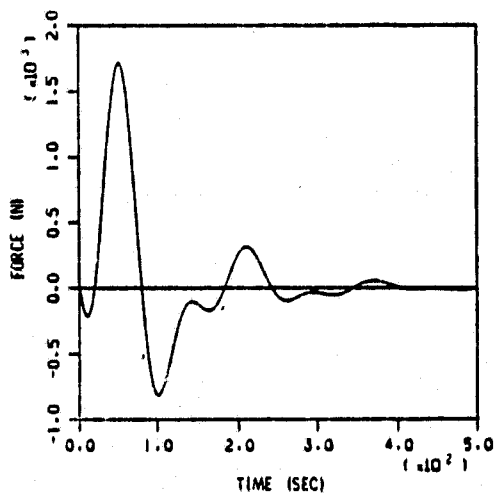
d) Mode 7
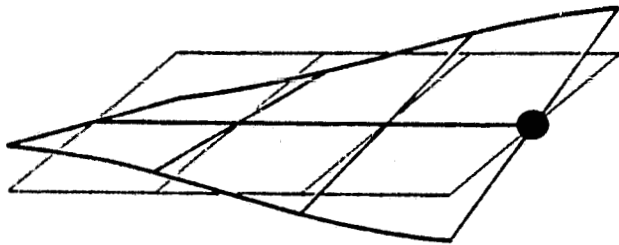
b) Mode 5
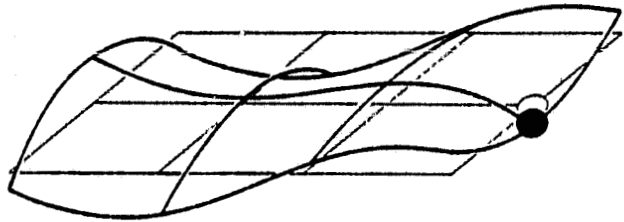
e) Mode 8

c) Mode 6

f) Mode 9

Figs. 3 Mode shapes of the first six flexible modes of the unrestrained plane grillage
structure (diagonal members not included in figures)
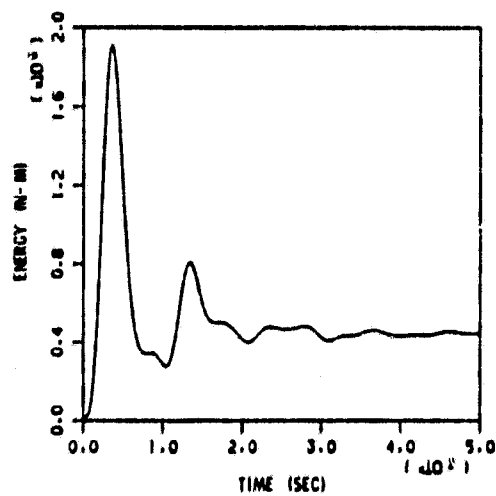
a) Total energy
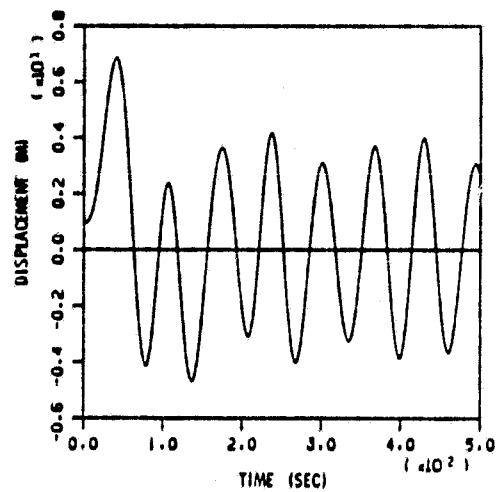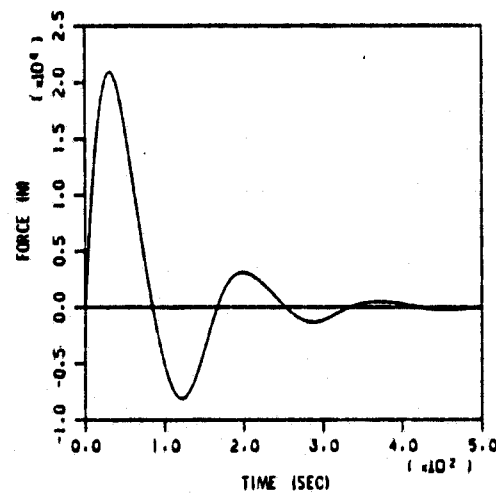
b) Translation of node 2

c) Control force at node 2

Figs. 4 Case 1: control thrusters 1, 2, 3, 5, 10, 12; viscous damping with t_s = 400 s, p_s = 0.01
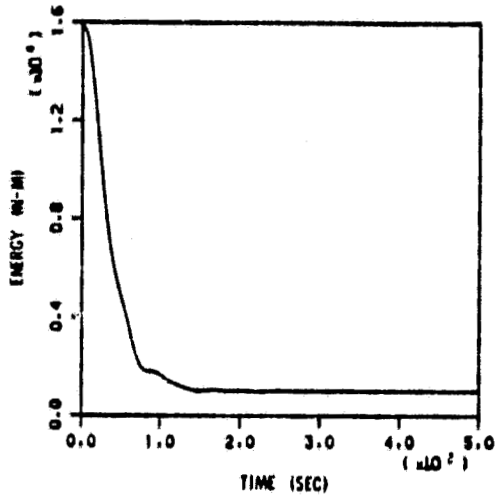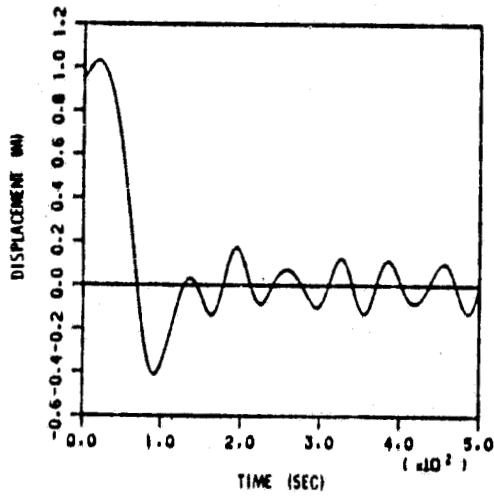

a) Total energy

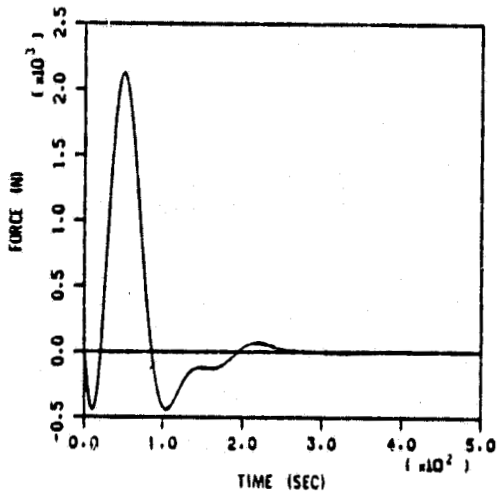b) Translation of node 2

c) Control force at node 2

Figs. 5 Case 2: control thrusters 1, 2, 3, 10, 11, 12; viscous damping with t_s = 400 s, p_s = 0.01
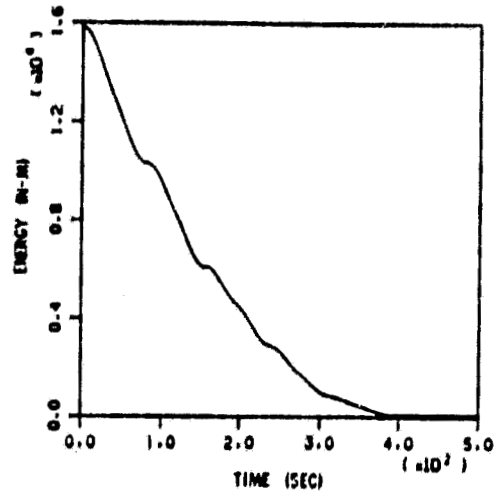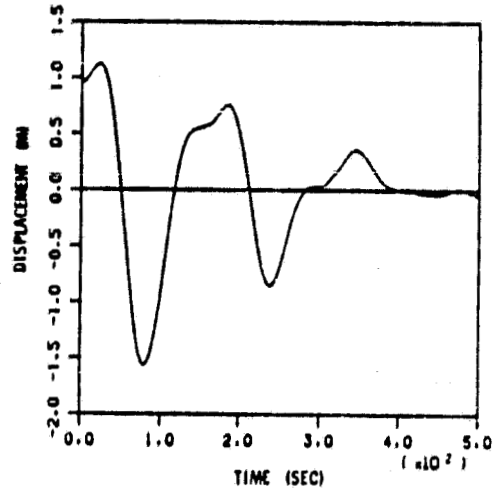
10

20

a) Total energy

a) Total energy

b) Translation of node 2

b) Translation of node 2

c) Control force at node 2

c) Control force at node 2

Figs. 6 Case 3: control thrusters 1, 2, 3, 5, 10, 12; viscous damping with t_s = 200 s, p_s = 0.01
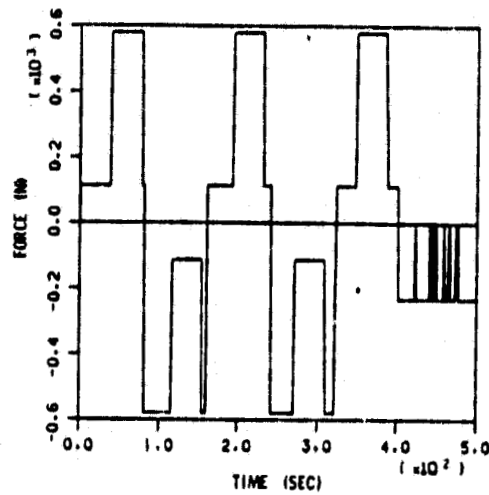
Figs. 7 Case 4: control thrusters 1, 2, 3, 5, 10, 12; Coulomb damping with t_s = 400 s, ϵ_v = 0.0001 m/s

11

APPENDIX B

B.1 IDEAL FORCE APPORTIONING

(This section is intended to be the replacement for Section V of Ref. 2.
Accordingly, the section title number, equation numbers, and reference numbers are those of Ref. 2.)

V. IDEAL FORCE APPORTIONING

We define "controlled" modes as being the m modes described by the index s in Eqs. (10) and (15). Although this set has been defined previously as consisting only of the target modes, it is clear now, in view of Eq. (22), that the set of m modes should include not only the flexible target modes, but also all appropriate rigid body modes. It is assumed in the following that the m controlled modes are specified.

In order to establish a mathematically ideal force apportioning vector f_s for a single controlled mode (denoted by subscript s), we define $Q_s(t) = f_s \, g(\dot{\xi}_s)$, where $g(\dot{\xi}_s)$ represents the feedback time dependence described in Eqs. (5) and (11). It is generally possible to provide control forces at only a few translation d.o.f. of a discretized structure. Hence, the $n \times 1$ vector f_s must usually include mostly zero elements. We therefore denote the actual number of control thrusters (actuators) positioned on the structure as n_a, and the corresponding $n_a \times 1$ force apportioning vector as f_s^a, the elements of which should generally be non-zero. Accordingly, the $n_a \times 1$ partition of modal vector ϕ_r corresponding to the control actuator d.o.f. is denoted ϕ_r^a. Therefore, Eq. (3) becomes

$$M_r \ddot{\xi}_r + M_r \omega_r^2 \xi_r = (\phi_r^a, \, f_s^a) \, g(\dot{\xi}_s), \quad r = 1, 2, \ldots, n \qquad (23)$$

It is necessary in the present context to choose the number of control actuators equal to the number of modes to be controlled, $n_a = m$. Then the m

22

equations of (23) which describe the controlled modes can be written in matrix form as

$$[M^c]\ddot{\xi}^c + [\omega^2 M^c]\xi^c = [\phi^{ac}]^T f_s^a \, g(\dot{\xi}_s) \tag{24}$$

where $[M^c]$, $[\omega^2 M^c]$, and $[\phi^{ac}]$ are appropriate m x m partitions of the n x n generalized mass, generalized stiffness, and modal matrices, respectively.

To decouple controlled mode s from all other controlled modes in Eq. (24), we seek f_s^a such that only the modal equation for mode s has a non-zero right-hand side. Clearly, this objective is achieved by setting

$$f_s^a = \psi_s \tag{25}$$

where ψ_s is the column vector corresponding to controlled modes of the matrix

$$[\psi] = [\phi^{ac}]^{-T} \tag{26}$$

In calculations, f_s^a is normalized to a maximum element absolute value of 1, as are all mode shape vectors. Provided that $[\phi^{ac}]$ is not singular, then the entire apportioning matrix of Eq. (26) can be calculated; then the set of vectors f_s^a, s = 1, 2, ... m, from Eq. (25) decouples the m equations of the controlled modes in modal Eqs. (10) or (15), but leaves the remaining n-m equations of the uncontrolled (residual) modes excited by the controlled modes. An important objective in control thruster selection, therefore, is to minimize excitation of the uncontrolled modes.

The apportioning procedure described in this section requires complete modal information on the controlled modes, and it assures that each of the controlled modes can be isolated from all other controlled modes. On the other hand, apportioning techniques used in modal testing[5-8] do not require modal parameters a priori, but they also do not produce any assured measure of mode isolation. So the apportioning calculated by Eqs. (25) and (26)

23

represents a mathematically ideal apportioning of a limited number of control thrusters, but it may not be best in practice because it requires previously determined modal parameters.

B.2 NON-IDEAL FORCE APPORTIONING BY MATRIX PSEUDO-INVERSE

We begin with a somewhat more explicit derivation of the results of Eqs. (25) and (26) above. The complete $m \times m$ force apportioning matrix is defined to be

$$[F^a] = [\underline{f}_1^a, \ldots, \underline{f}_m^a] \tag{B.2.1}$$

To uncouple all controlled modes, we seek $[F^a]$ such that (see Eq. (24) above)

$$[\phi^{ac}]^T [F^a] = [I_m] \tag{B.2.2}$$

where $[I_m]$ is the $m \times m$ identity matrix. Clearly,

$$[F^a] = [\phi^{ac}]^{-T} \tag{B.2.3}$$

In our computations for $\underline{f}_s^a$, $s = 1, 2, \ldots, m$, each column of $[F^a]$ is subsequently normalized to a maximum element absolute value of 1.

In practice, it will probably be desirable to control a greater number of modes than there are control actuators, $m > n_a$. For this situation, we define the force apportioning matrix $[F^a]$ just as in Eq. (B.2.1), except that now each column has length n_a. We again seek the solution of Eq. (B.2.2), where now $[\phi^{ac}]$ is an $n_a \times m$ matrix. Since the unknowns in this equation are overdetermined, a unique, exact solution does not generally exist. We proceed formally as follows:

24

$$[\phi^{ac}] [\phi^{ac}]^T [F^a] = [\phi^{ac}] [I_m]$$

$$[F^a] = ([\phi^{ac}] [\phi^{ac}]^T)^{-1} [\phi^{ac}] \tag{B.2.4}$$

Error $\underset{\sim}{e}_j$ is defined as the jth column of $[\phi^{ac}]^T [F^a] - [I_m]$. Then Eq. (B.2.4) represents the least-squares approximate solution of Eq. (B.2.2) for $m > n_a$, for which each norm $(\underset{\sim}{e}_j, \underset{\sim}{e}_j)$, $j = 1, 2, \ldots, m$, is a minimum.[*] Eq. (B.2.4) clearly reduces to Eq. (B.2.3) if $m = n_a$. Eq. (B.2.4) is a form of the so-called matrix pseudo-inverse for the overdetermined least-squares case. If it is desired to weight the control of certain modes over control of others, a generalization of Eq. (B.2.4) for a weighted least-squares approximate solution is easily developed.[*]

---

[*] W. L. Brogan, Modern Control Theory, pp. 90-92, Quantum Publishers, 1974.

APPENDIX C

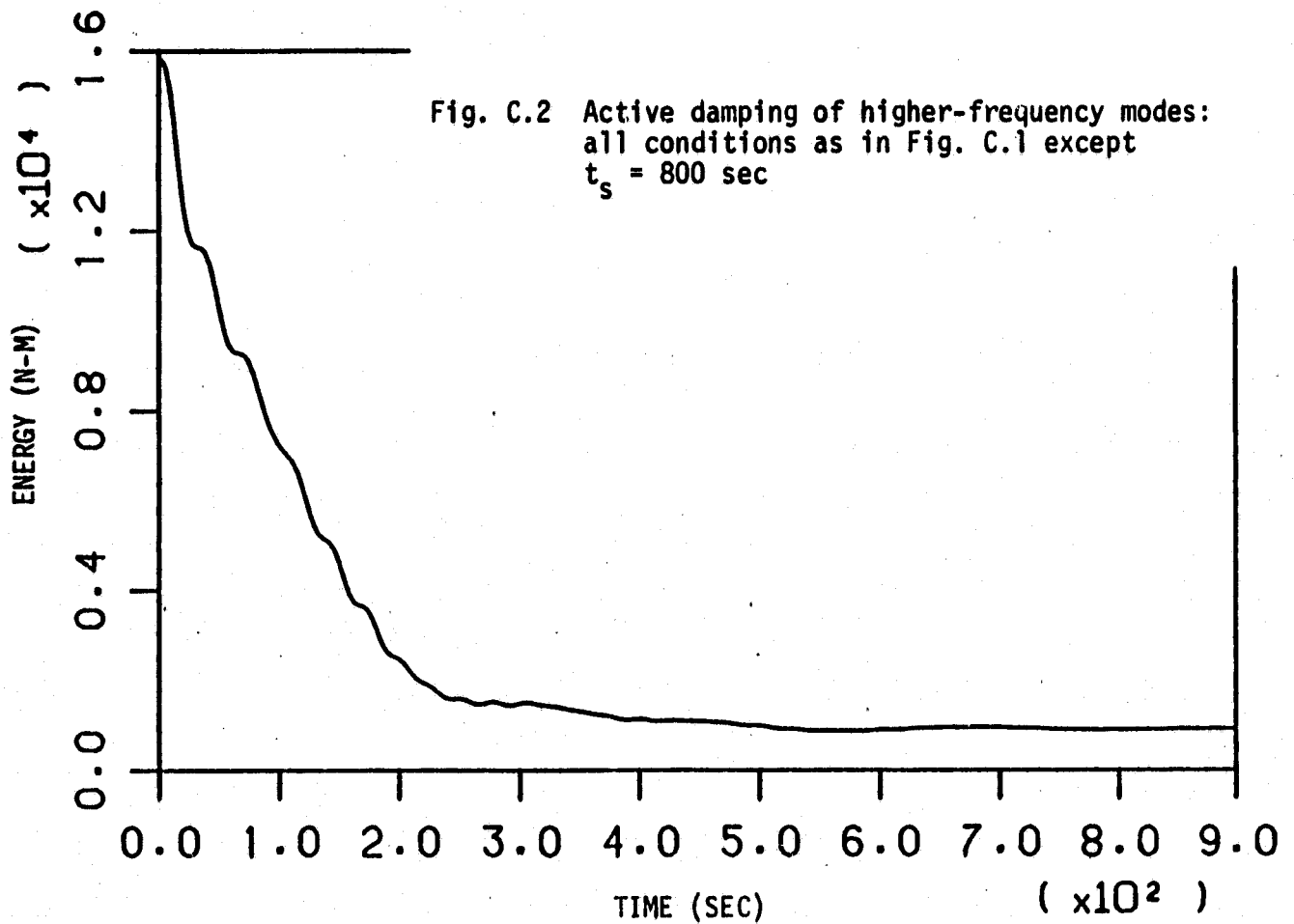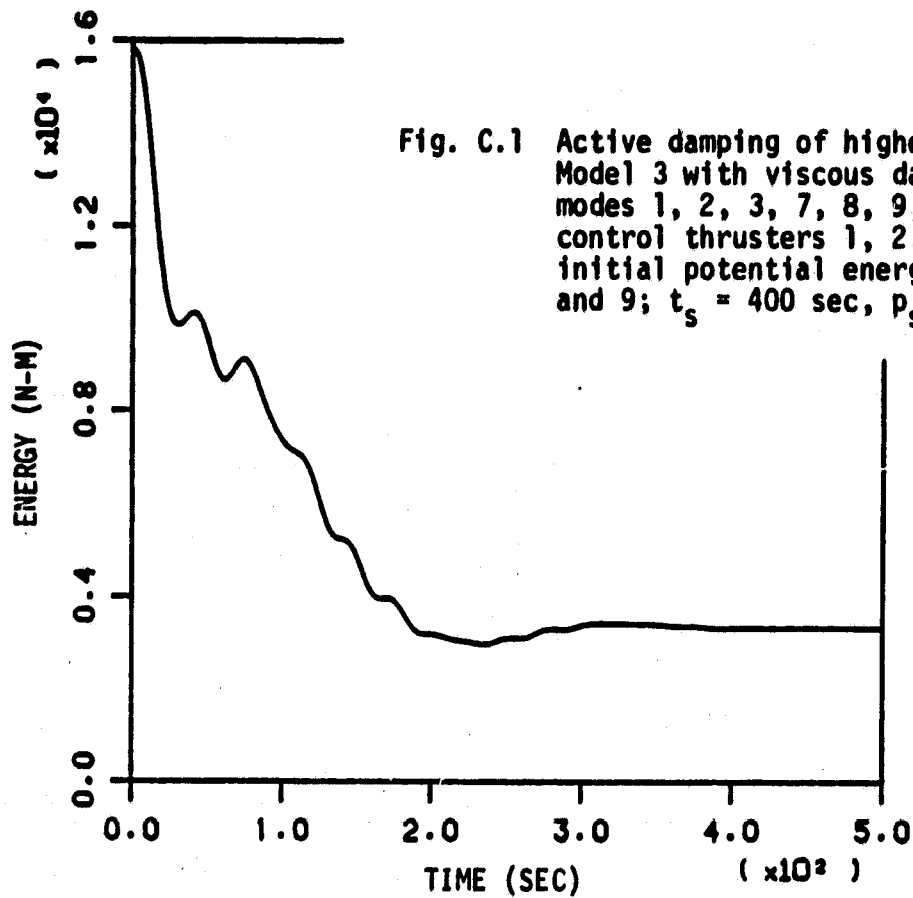## ACTIVE DAMPING OF HIGHER-FREQUENCY MODES

A single case was investigated, the numerical simulation model being the unrestrained plane grillage described in Ref. 2. The target modes were specified to be modes 7, 8, and 9 (rather than modes 4, 5, and 6, as in Ref. 2), and the controlled modes were specified to be the target modes plus the rigid body modes, modes 1, 2, and 3.

Twenty-five combinations of six control thruster locations were considered in a trial-and-error search for the combination producing the least excitation of the uncontrolled modes. The combination of thrusters 1, 2, 3, 5, 10, 12, which is quite effective if nodes 4, 5, and 6 are the target modes (cf. Ref. 2), was found to be very poor for target modes 7, 8, and 9. The most effective combination for this case (among those investigated) consists of control thrusters 1, 2, 3, 7, 9, 11 (cf. Fig. 2 of Ref. 2), and this combination was used in time history numerical simulations of active damping.

Viscous-type damping was used. The initial conditions specified correspond to an equal amount of initial potential energy in each of the target modes, with zero initial kinetic energy in the target modes, and zero initial energy in all non-target modes. The feedback signal used was node 1 translation velocity $\dot{q}_1(t)$. The exact force apportioning vectors (Eq. (29) of Ref. 2) were used, and filtering was taken to be ideal.

Figures C.1 and C.2 are energy-decay time histories comparable to Figs. 4a-7a of Ref. 2. With specified time $t_s = 400$ s to damp each target mode down to portion $p_s = 0.01$ of its initial amplitude, the residual energy shown on Fig. C.1 is about 21% of the initial energy. About half of the residual energy resides in each of modes 6 and 10, the modes immediately adjacent to

26

the target modes. Figure C.2 shows that the doubling of specified damping time to 800 s produces a much more satisfactory final residual energy of 6% of the initial energy.

Fig. C.1 Active damping of higher-frequency modes: Model 3 with viscous damping; controlled modes 1, 2, 3, 7, 8, 9, target modes 7-9; control thrusters 1, 2, 3, 7, 9, 11; equal initial potential energy in modes 7, 8, and 9; $t_s = 400$ sec, $p_s = 0.01$

Fig. C.2 Active damping of higher-frequency modes: all conditions as in Fig. C.1 except $t_s = 800$ sec

APPENDIX D

INEXACT MODAL PARAMETERS FOR THE CONTROLLED STRUCTURE

We have investigated this subject primarily by doing numerical experiments, i.e., computer simulations of active damping, rather than a theoretical study. Our first step was to define a "model" structure and an "actual" structure, both of which are really just mathematical models. The "errors" in the "model" structure relative to the "actual" structure are small differences in the mass distributions. These "errors" are presumably typical of the inaccuracies which inevitably exist in a finite element model relative to the real structure.

Following definition of the "model" and "actual" structures and calculation of the vibration modes for both, the ideal force apportioning vectors were calculated by Eqs. (28) and (29) of Ref. 2 from the modal matrix of the "model" structure. Finally, these force apportioning vectors were used in numerical simulations of active damping on the "actual" structure. The quality of the active damping then was an indication of the effect of non-ideal force apportioning, which results from inexact modal parameters. A short digression on the theory is appropriate before presentation of numerical results.

The mathematical consequence of non-ideal force apportioning is to produce non-zero inner products (ϕ_r, f_s) for $r \neq s$ in the modal equations of the controlled modes (those modes denoted by the index s in Eqs. (10) and (15) of Ref. 2), thus coupling the controlled modes. It is to be expected, then, that active damping with non-ideal force apportioning will be less effective than active damping with ideal force apportioning. Moreover, the coupling of controlled modes could conceivably lead to their instability, which is not possible without coupling. Nevertheless, most of the numerical simulations to be described next exhibit neither substantial damping degradation nor instability.

29

The "actual" structure considered here (referred to as Model 5) is slightly different than the structure described in Ref. 2 (referred to as Model 3), for reasons to be given below. Model 5 is identical to Model 3 in geometry and mass distribution, and its stiffness distribution is the same in all respects except that its center longitudinal member (conne 'ing nodes 2, 5, 8, and 11 in Fig. 2 of Ref. 2) has a greater torsional stiffness, $GJ = 2.0 \times 10^{14}$ N·m^2. This stiffening separates mode 5, the first flexible torsion mode, from mode 4, the first flexible bending mode (cf. Figs. 3 and Table 1 of Ref. 2); mode 5 natural frequency of Model 5 is 0.0097 Hz, in contrast to 0.0065 Hz for Model 3. The frequencies of bending modes 4 and 6 are identical for the two models.

The "model" structure considered is identical to the "actual" structure except that it has additional small lumped masses at nodes 8, 10, and 11* (cf. Fig. 2 of Ref. 2); each has mass of 2.0×10^5 kg and rotational inertias of 8.0×10^9 kg·m^2. The effects of these mass perturbations are to make the "model" structure's lowest natural frequencies on the order of 10% lower than those of the "actual" structure, and also to alter the mode shapes somewhat.

Ideal force apportioning vectors were calculated for both the "actual" and "model" structures, with the controlled modes specified as modes 1-6 and the control thruster locations specified as nodes 1, 2, 3, 5, 10, and 12. These vectors are listed for target modes 4, 5, and 6 in Table D.1. Comparison of the vectors for "actual" and "model" structures shows that those for bending modes 4 and 6 are quite similar, while those for torsion mode 5 differ substantially.

_____

*It would be more natural if the "model" structure were symmetric and the "actual" structure had the asymmetric mass perturbations, but it proved convenient in computations to proceed as described above.

Energy time histories for viscous and Coulomb active damping are shown in Figs. D.1 and D.2, respectively. Simulations for both ideal and non-ideal apportionings were run to provide a comparison. Viscous damping with the non-ideal apportioning is, surprisingly, slightly better than that with ideal apportioning. Coulomb damping with non-ideal apportioning produces a slightly faster decay but also excites slightly more residual energy than that with ideal apportioning.

The results in Figs. D.1 and D.2 are representative of a number of similar cases investigated in which the modes of the "model" structure are not substantially different from those of the "actual" structure. The invariable observation was that non-ideal apportioning resulting from inexact modal parameters produces a slightly different damping character than does ideal apportioning, but never any serious degradation of short-term damping quality nor any noticeable long-term instability. The conclusion then is that the quality of active damping by force apportioning is not very sensitive to small errors in modal parameters of the controlled modes.

However, it is not valid to state that active damping quality is always insensitive to small errors in the primitive physical parameters (i.e., stiffness and mass distributions) of the controlled structure; the existence of closely spaced modes (high modal density) can cause problems. To illustrate this, we evaluated a case for which Model 3 is the "actual" structure, and the "model" structure differs only in the presence of a small lumped mass at node 10. An important effect of this small additional mass is to reverse the characters of the two closely spaced, lowest flexible modes of the "model" structure relative to the same modes of the "actual" structure (cf. Table 1 and Figs. 3 of Ref. 2): mode 4 of the "model" structure is torsion, and mode 5 is bending.

31

Because like-numbered mode shapes of the "actual" and "model" structures are fundamentally different in this case, active damping of the "actual" structure by force apportioning calculated for the "model" structure produces very poor results. For this particular example, the problem can be solved simply by reversing the order of mode shapes 4 and 5 in the modal matrix of the "model" structure before calculating the force apportioning vectors.* In general, however, the existence of substantial errors in estimates of mode shapes can seriously degrade the quality of active damping by force apportioning. It seems probable that actual hardware implementation of this or any other scheme for active vibration control of large space structures will require an adaptive capability.

_____

*Nevertheless, we considered it desirable to avoid this confusing complication by using Model 5, which has well separated first bending and torsion modes, for the principal numerical examples of this appendix.

Table D. 1 Ideal Force Apportionings

Thruster	"Actual" Structure Mode			"Model" Structure Mode		
	4	5	6	4	5	6
1	-0.13	1	0.57	-0.18	0.15	0.59
2	0.92	0	-1	0.95	0.90	-1
3	-0.13	-1	0.57	-0.11	-1	0.54
5	-1	0	-0.21	-1	-0.07	-0.18
10	0.17	-1	0.03	0.20	-0.56	0.01
12	0.17	1	0.03	0.13	0.59	0.06
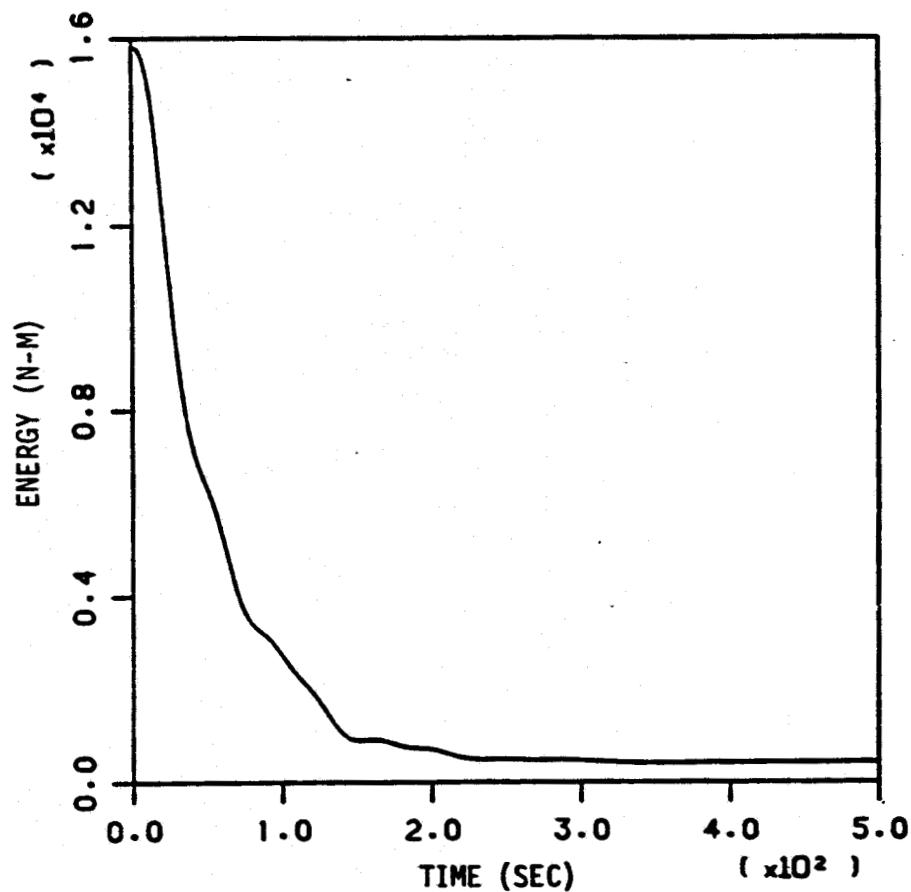
(a) Force apportioning for the "actual" structure
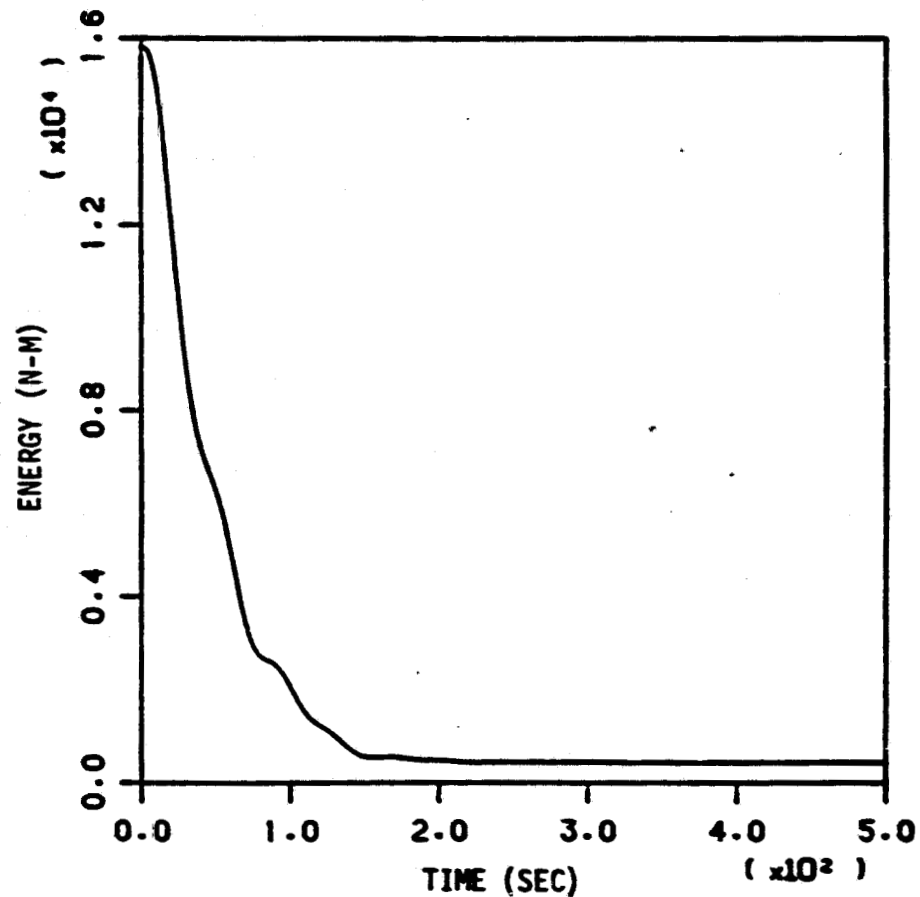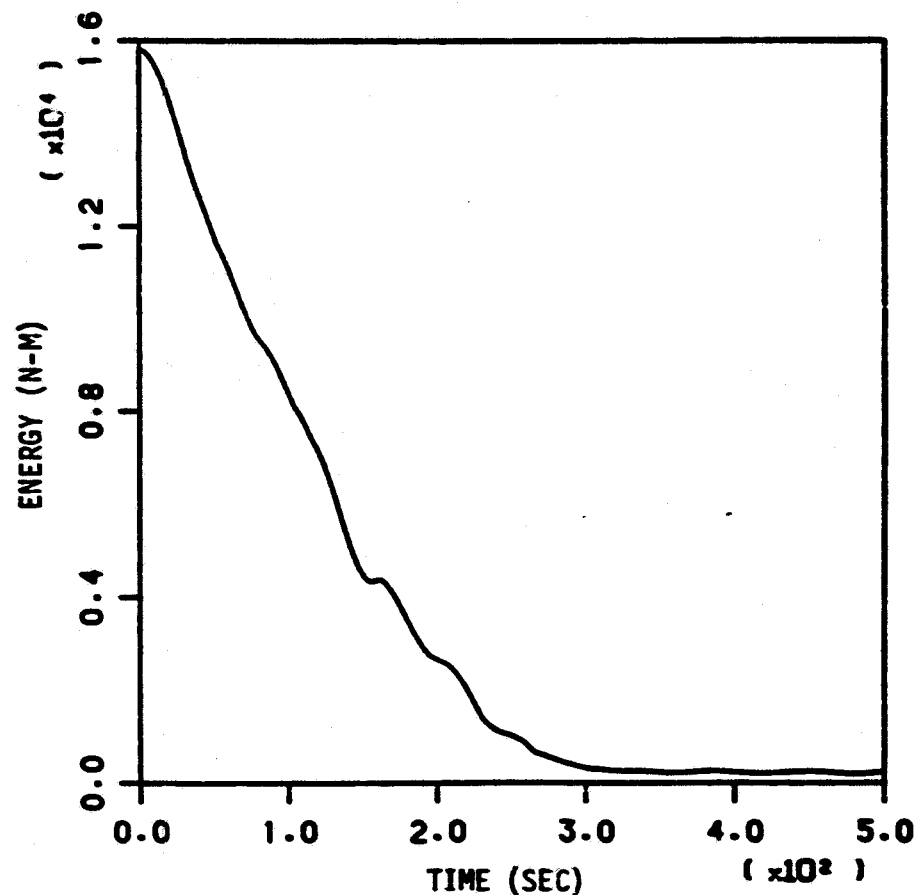
(b) Force apportioning for the "model" structure

Fig. D.1 The effect of non-ideal force apportioning on damping of the "actual" structure: Model 5 with viscous damping; controlled modes 1-6, target modes 4-6; control thrusters 1, 2, 3, 5, 10, 12; equal initial potential energy in modes 4, 5, and 6; t_s = 400 sec, p_s = 0.01

34
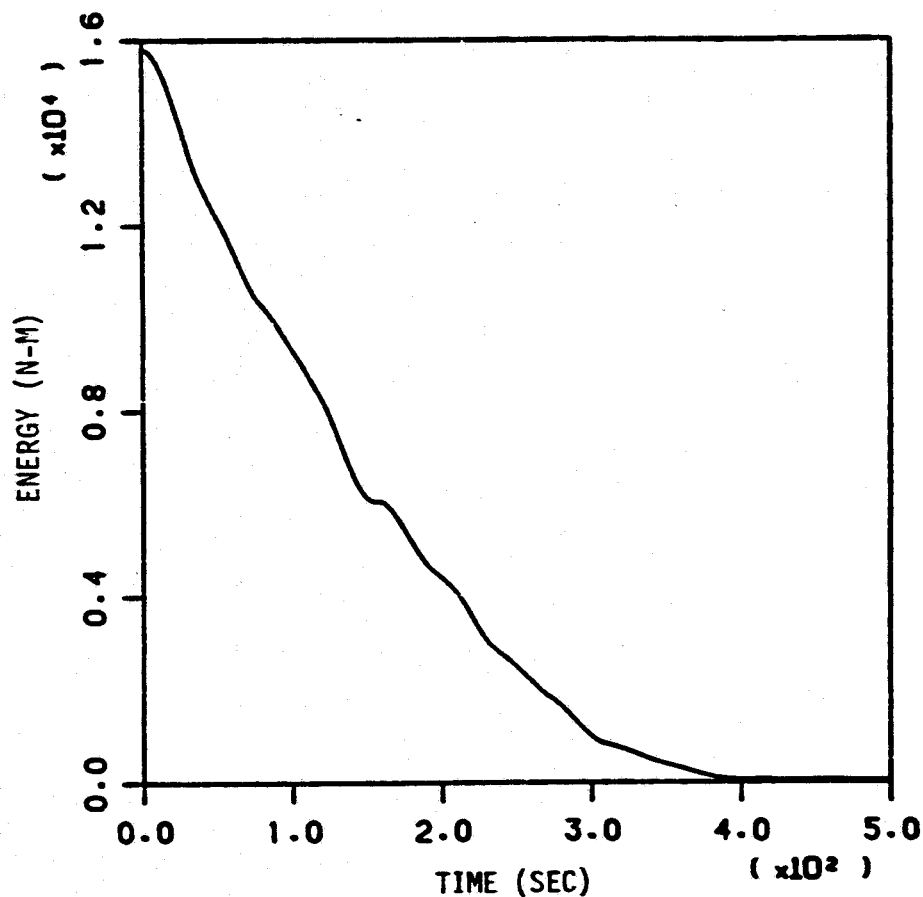
(a) Force apportioning for the "actual" structure

(b) Force apportioning for the "model" structure

Fig. D.2   The effect of non-ideal force apportioning on damping of the "actual" structure: Model 5 with
Coulomb damping; controlled modes 1-6, target modes 4-6; control thrusters 1, 2, 3, 5, 10, 12;
equal initial potential energy in modes 4, 5, and 6; t_s = 400 sec, ε_v = 0.0001 m/sec

APPENDIX E

NON-IDEAL FREQUENCY FILTERING

Equations (10) and (11) of Ref. 2 can be written as

$$M_r \ddot{\xi}_r + M_r \omega_r^2 \xi_r = - \sum_{s=1}^{m} K_s(\pmb{\ell}_r, \pmb{f}_s) h(\dot{q}_{is}),$$

$$r = 1, 2, \ldots, n \tag{E.1}$$

where

$$h(\dot{q}_{is}) = \begin{cases} \dot{q}_{is} & \text{for viscous damping} \\ sgn(\dot{q}_{is}) & \text{for Coulomb damping} \end{cases}$$

The term $\dot{q}_{is}$ in Eq. (E.1) implies ideal filtering at each controlled mode natural frequency ω_s, $s = 1, 2, \ldots, m$, as is illustrated conceptually on Fig. 1 of Ref. 2. The ideal filter for controlled mode s passes only the $\dot{q}_{is}$ spectral component of the total sensor velocity, $\dot{q}_i = \sum_{r=1}^{n} \dot{q}_{ir}$. The ideal filter, then, has an infinitely narrow pass-bank and infinitely steep rolloff rates. Since $\dot{q}_{is} = \phi_{is} \dot{\xi}_s$, a mathematical characteristic of ideal filtering is that it does not couple the controlled modes in Eq. (E.1). Those modes might be coupled if non-ideal force apportioning is used with ideal filtering, but in such a case the non-ideal apportioning is responsible for the coupling. If both apportioning and filtering are ideal, then the controlled modes are not coupled at all.

On the other hand, a non-ideal, more realistic filter has a finite pass-band and finite rolloff rates, and it consequently passes spectral components of all frequencies. The characteristics of a non-ideal filter for controlled mode s are illustrated on Fig. E.1. For such a filter, the function $h(\dot{q}_{is})$ in Eq. (E.1) must be replaced by a filter output function

$$F_{is} = \sum_{j=1}^{n} A_{sj} h(\dot{q}_{ij}), \quad s = 1, 2, \ldots, m$$

36

where constants A_{sj} are attenuation factors illustrated in Fig. E.1. For ideal filtering, $A_{sj} = \delta_{sj}$, the Kronecker delta. Calculation of the attenuation factors for non-ideal filtering is discussed below. For non-ideal filtering, then, the modal equations have the form

$$M_r \ddot{\xi}_r + M_r \omega_r^2 \xi_r = -\sum_{s=1}^{m} K_s(\ell_r, f_s) \sum_{j=1}^{n} A_{sj} h(\phi_{1j} \dot{\xi}_j),$$

$$r = 1, 2, \ldots, n \qquad (E.2)$$

In Eq. (E.2), both controlled and uncontrolled modes are coupled by the non-ideal filtering, regardless of the type of force apportioning used. So it is to be expected that non-ideal filtering will reduce the effectiveness of active damping by force apportioning and, moreover, that it may even produce system instability due to the coupling. Nevertheless, numerical results presented below for typical non-ideal filter characteristics exhibit neither substantive degradation of damping quality nor instability.

To calculate constants A_{sj}, one must specify frequency cutoffs and rolloff rates. Filter rolloff rates are designated in terms of decibels per octave. So, for a high frequency rolloff at rate R db/oct, we have (see Fig. E.1)

$$20 \log_{10} A_{sj} = -R \log_2(\omega_j/\omega_{sh})$$

$$= -R \log_{10}(\omega_j/\omega_{sh})/\log_{10} 2$$

Solving for the attenuation factor gives,

$$A_{sj} = (\omega_j/\omega_{sh})^{-R/20 \log_{10} 2}, \quad \omega_j \geq \omega_{sh} \qquad (E.3a)$$

Similarly, for a low frequency rolloff,

$$A_{sj} = (\omega_j/\omega_{s\ell})^{R/20 \log_{10} 2}, \quad \omega_j \leq \omega_{s\ell} \qquad (E.3b)$$

37

We have run several numerical simulations of active damping by force apportioning with non-ideal filtering. The structural models used in these simulations are those described in Appendix D. Simulations with Model 3 tested the effect of non-ideal filtering alone, since ideal force apportioning was used, and simulations with Model 5 (as the "actual" structure) and the related "model" structure tested the effects of non-ideal filtering and non-ideal apportioning acting simultaneously. In all cases, modes 1-6 were specified as the controlled modes and modes 4-6 as the target modes, and control actuator locations were specified as nodes 1, 2, 3, 5, 10, and 12.

The filter cutoff frequencies specified for both Model 3 and Model 5 can be described with reference to Fig. E.2. A low-pass filter was used for mode 4, and band-pass filters were used for modes 5 and 6. The cutoff frequencies were selected to be

$$\omega_{4h} = \omega_{5\ell} = (\omega_4 + \omega_5)/2$$

$$\omega_{5h} = \omega_{6\ell} = (\omega_5 + \omega_6)/2 \tag{E.4}$$

$$\omega_{6h} = (\omega_6 + \omega_7)/2$$

The particularly interesting characteristic of Model 3 is the close proximity of natural frequencies 4 and 5 (cf. Table 1 of Ref. 2). This closeness might lead one to expect that non-ideal filtering would produce substantial coupling between modes 4 and 5 and, hence, would reduce the quality of damping.

To test this expectation, we ran Model 3 cases with filter rolloff rates varying from the unrealistically high value of 160 db/oct, through the practically realistic values of 80 and 48 db/oct, and down to the unrealistically low value of 10 db/oct. Cases were run with both viscous and Coulomb types of damping, and with different initial conditions.

The adverse effect of non-ideal filtering was found to be relatively small in all Model 3 cases with typical rolloff rates of 80 or 48 db/oct. The energy time history for the very worst of these cases investigated is shown in Fig. E.3, which may be compared with Fig. 4a of Ref. 2. Whereas ideal filtering was used for the latter, non-ideal filtering with 48 db/oct rolloff rate was used for the former; however, all other conditions were identical for the two runs. Comparison of the two figures shows that non-ideal filtering in this case retards the rate of active damping, but does not increase the final quantity of residual energy remaining in the structure.

Another Model 3 case of interest is one for which the unrealistically low rolloff rate of 10 db/oct was used. The energy time history is shown in Fig. E.4, which may be compared with Fig. 7a of Ref. 2. Ideal filtering was used for the latter and non-ideal filtering for the former, but all other conditions were identical for the two runs. Figure E.4 shows a short-term rate of damping very similar to that of Fig. 7a of Ref. 2. But the residual energy is greater in the case of non-ideal filtering; and, in fact, the energy increases after reaching a short-term minimum (at about 700 sec), strongly suggesting the presence of a system instability. This instability seems relatively weak and manifests itself only after the in-itially existing vibrations are essentially suppressed, so it might be regarded as a "long-term" instability.

Numerical simulations of active damping with Model 5 tested the sit-uation in which both the force apportioning and the filter cutoff frequencies[*] designed for the "model" structure were used for the "actual" structure.

_____

[*] The filter cutoff frequencies were designed for the "model" structure in accordance with Eqs. (E.4), with one exception: the high frequency cutoff for the Mode 6 filter had to be adjusted upward slightly for use with the "actual" structure, because the computer program requires the natural fre-quency to be within the pass-band.

Comparison of Figs. E.5a and E.5b shows that in this case the presence of both non-ideal apportioning and non-ideal filtering with a rolloff rate of 80 db/oct only slightly reduces the quality of active damping. The case was repeated for rolloff rates of 48 and 24 db/oct, with almost no further deterioration of damping quality. One additional halving of the rolloff rate, to the unrealistically low value of 12 db/oct, resulted in the energy time history of Fig. E.5c, which exhibits both substantative loss of short-term damping quality and long-term instability. Finally, a Model 5 case was run for which the rolloff rate was set to 0 db/oct, i.e., no filtering at all. For this case, the entire system, consisting of both controlled and uncontrolled modes, is strongly unstable.

To summarize and reiterate the observations made relative to non-ideal filtering in the particular cases studied: (1) the quality of active damping is not substantively decreased by typical filter characteristics; (2) both poor damping quality and long-term instability may occur ⌄r filtering with unusually low rolloff rates.
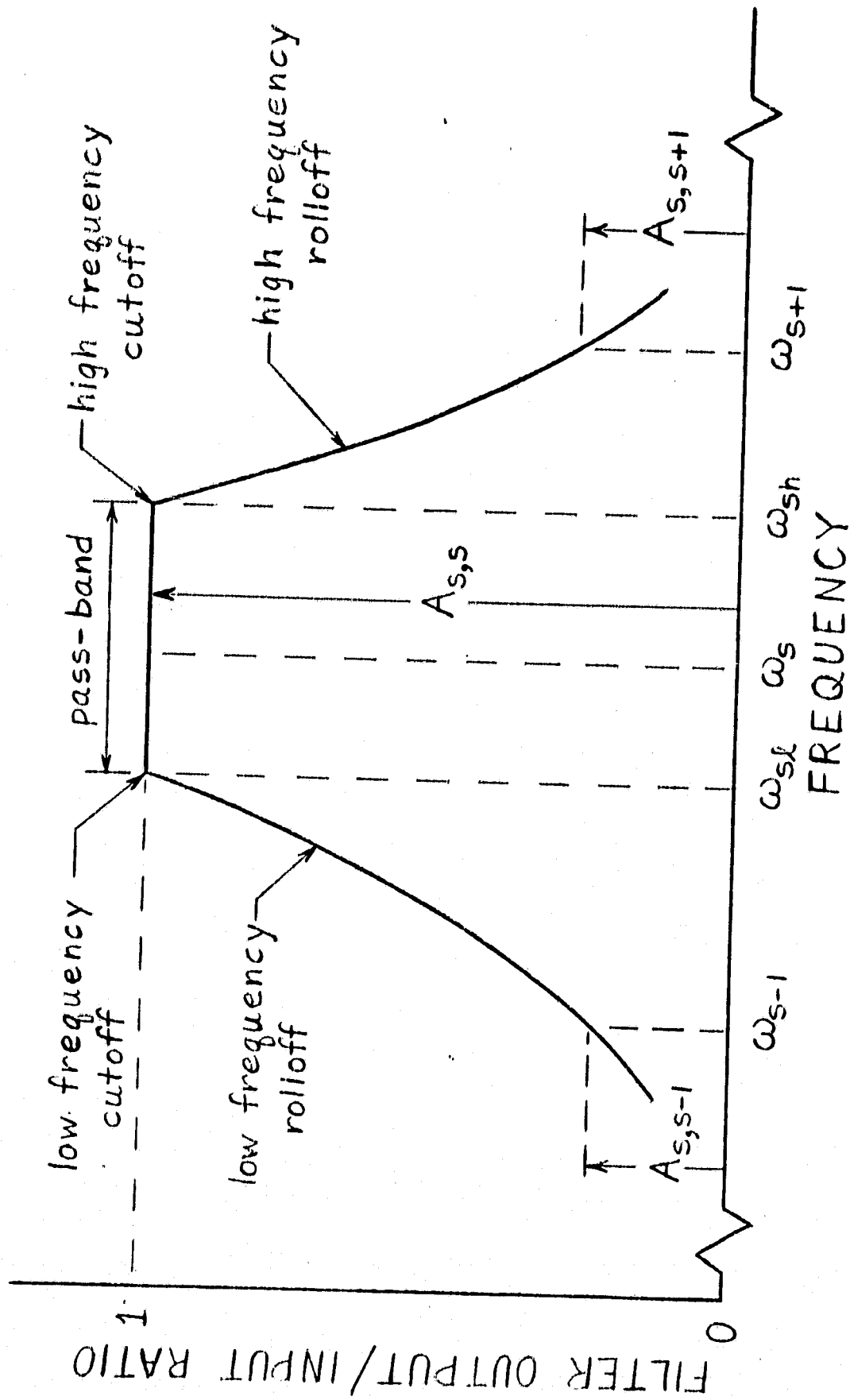
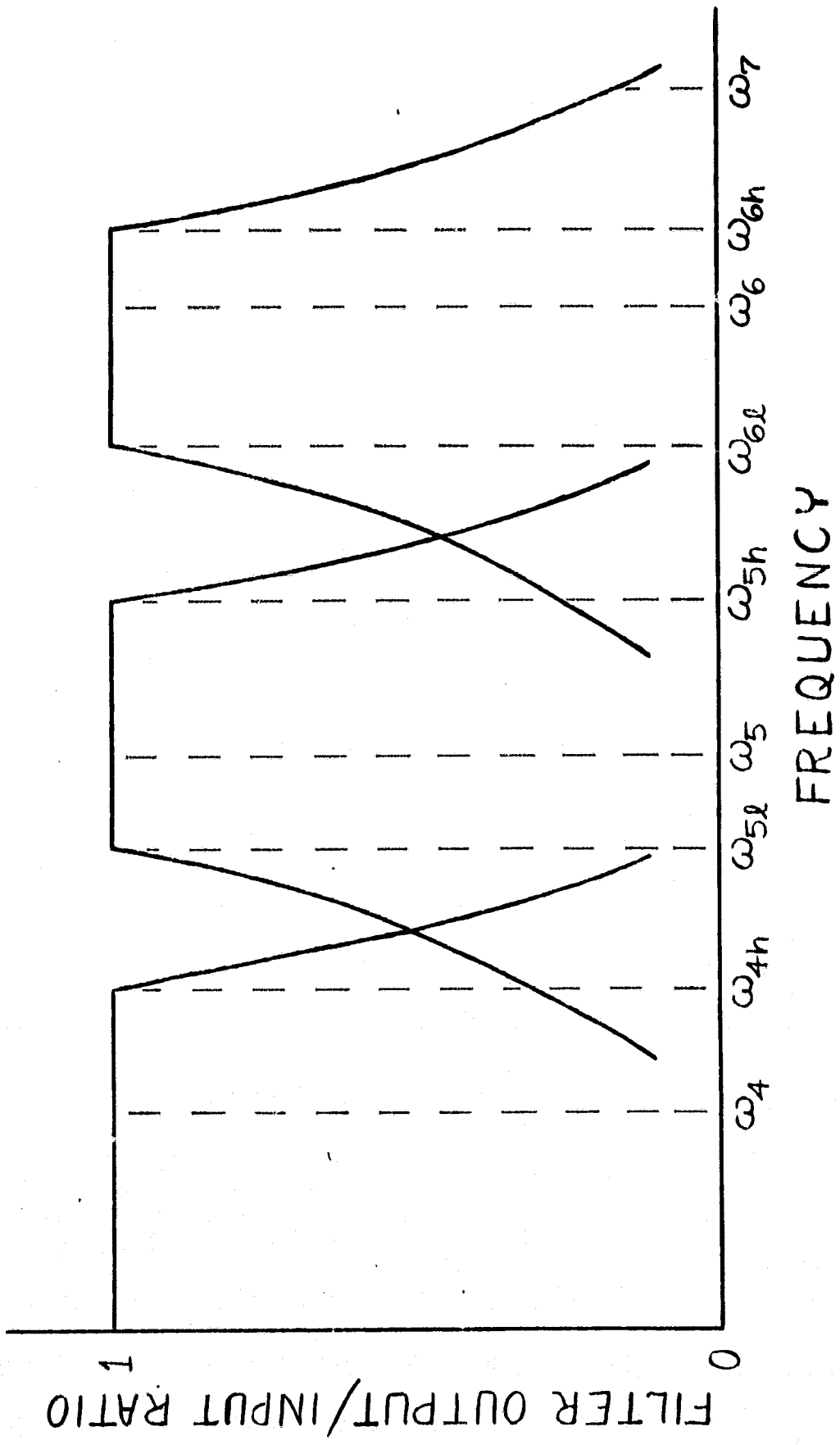Fig. E.1 Characteristics of non-ideal filter for controlled mode s

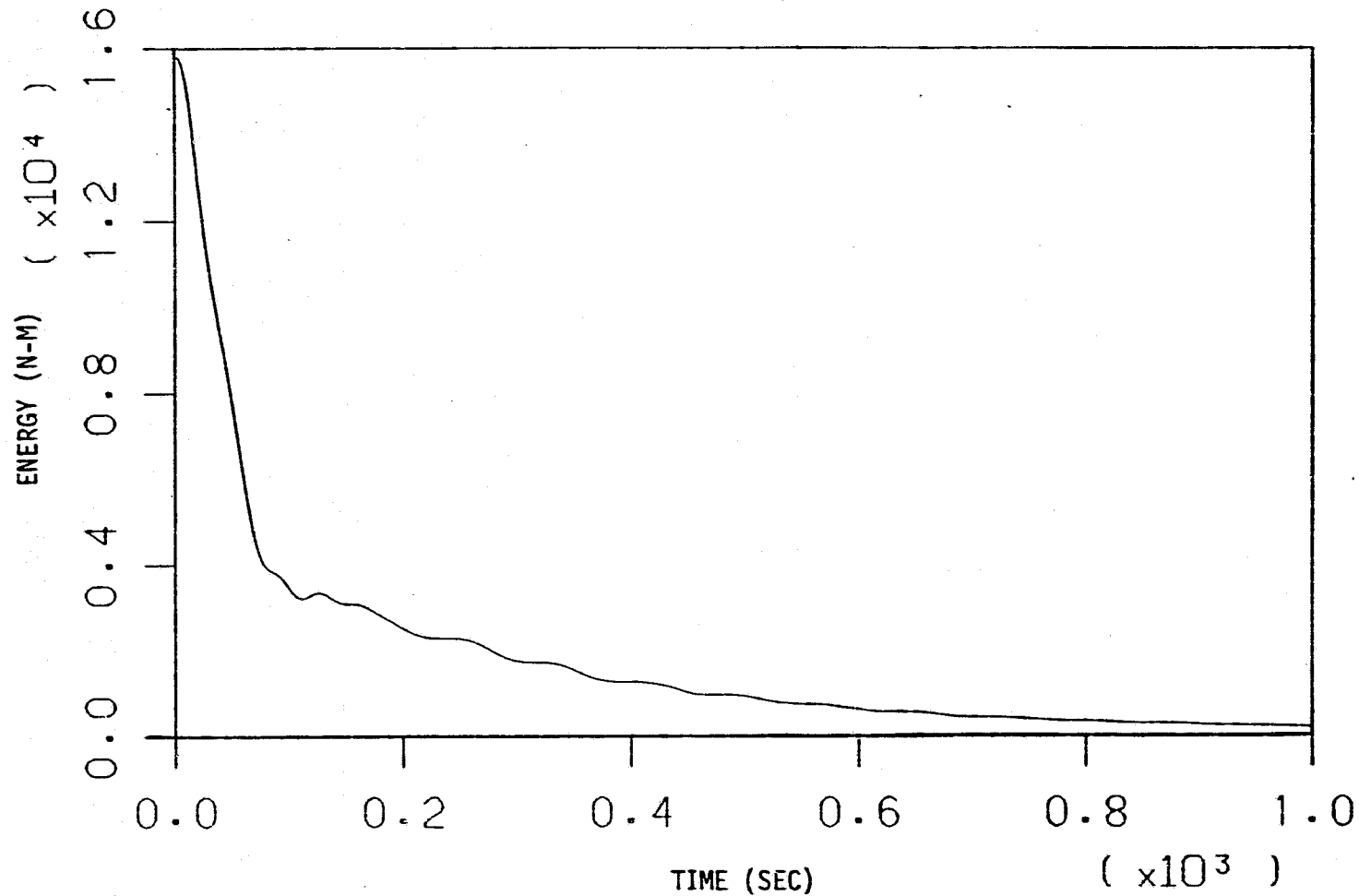Fig. E.2 Cutoff frequencies of target mode filters

Fig. E.3 The effect of non-ideal filtering: Model 3 with viscous damping; non-ideal filters with 48 db/oct rolloff rate, cutoff frequencies (Hz) of 0.00638 for mode 4 low-pass, 0.00638 and 0.00974 for mode 5 band-pass, 0.00974 and 0.01363 for mode 6 band-pass; controlled modes 1-6, target modes 4-6; control thrusters 1, 2, 3, 5, 10, 12; equal initial potential energy in modes 4, 5, and 6; t_s = 400 sec, p_s = 0.01
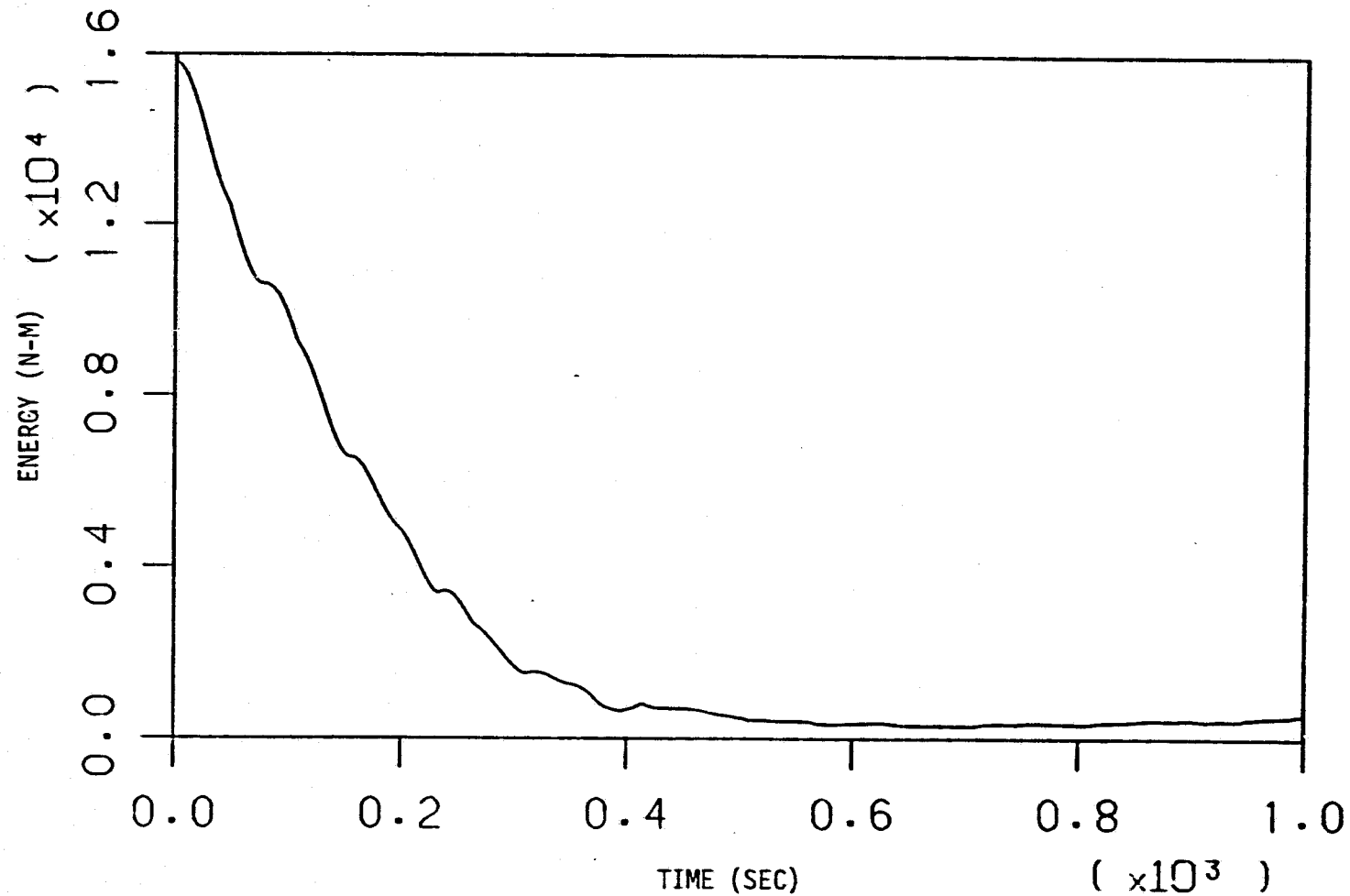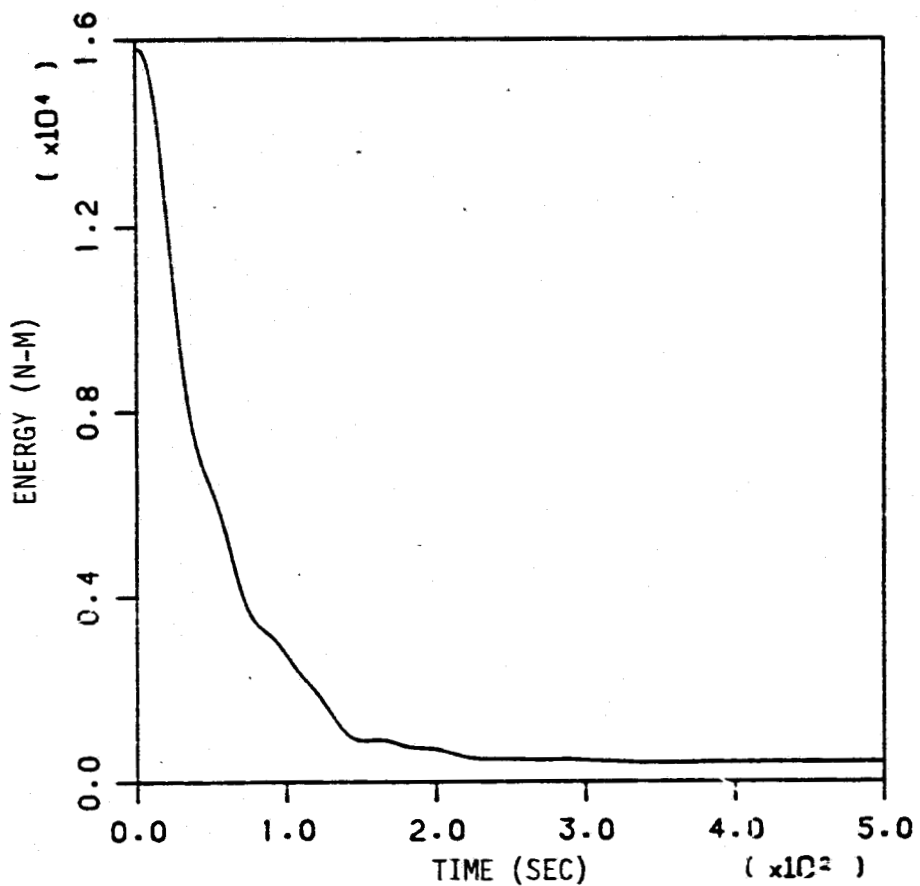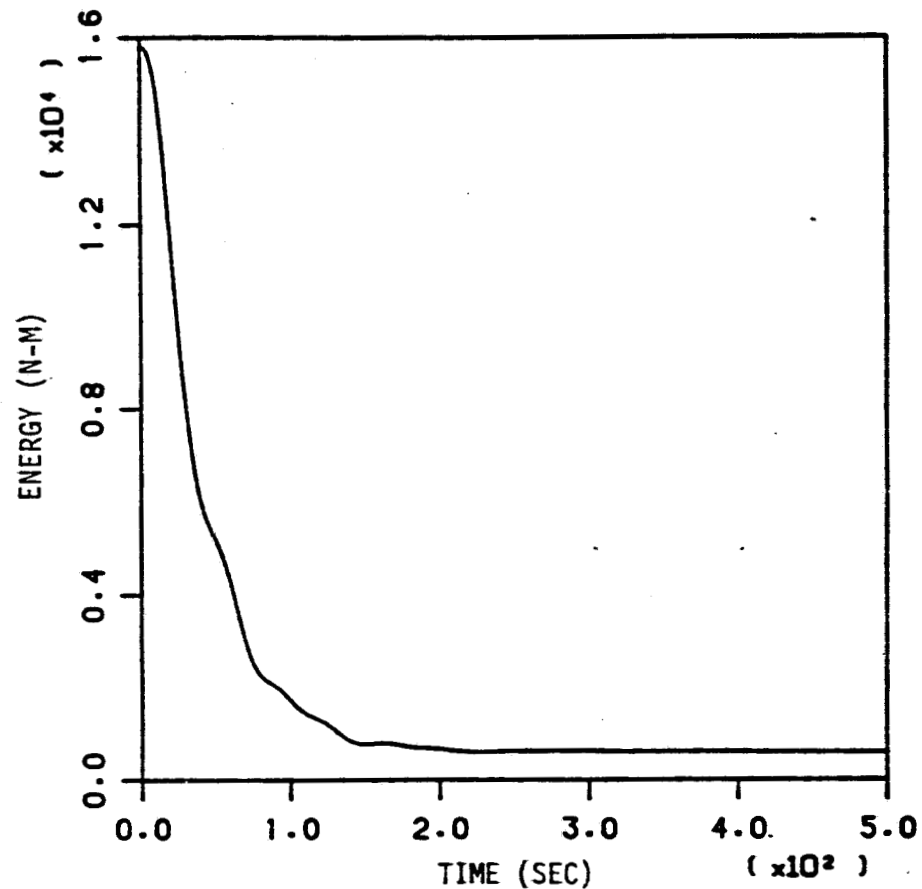
Fig. E.4 The effect of non-ideal filtering: Model 3 with Coulomb damping; non-ideal filters with 10 db/oct rolloff rate, cutoff frequencies (Hz) of 0.00638 for mode 4 low-pass, 0.00638 and 0.00974 for mode 5 band-pass, 0.00974 and 0.01363 for mode 6 band-pass; controlled modes 1-6, target modes 4-6; control thrusters 1, 2, 3, 5, 10, 12; equal initial potential energy in modes 4, 5, and 6; t_s = 400 sec, ε_v = 0.0001 m/sec

(a) Ideal filtering, and force apportioning for the "actual" structure

(b) Non-ideal filtering with 80 db/oct rolloff rate, and force apportioning for the "model" structure

Fig. E.5 The effects of both non-ideal apportioning and non-ideal filtering on damping of the "actual" structure: Model 5 with viscous damping; filter cutoff frequencies (Hz) of 0.00713 for mode 4 low-pass, 0.00713 and 0.01029 for mode 5 band-pass, 0.01029 and 0.01294 for mode 6 band-pass; controlled modes 1-6, target modes 4-6; control thrusters 1,2,3,5,10,12; equal initial potential energy in modes 4, 5, and 6; $t_s = 400$ sec, $p_s = 0.01$